

2 Percolation I

Armin Bunde and Shlomo Havlin

2.1 Introduction

Percolation represents the simplest model of a disordered system [2.1–10]. Consider a square lattice, where each site is occupied randomly with probability p or is empty with probability $1 - p$ (see Fig. 2.0). Occupied and empty sites may stand for very different physical properties. For simplicity, let us assume that the occupied sites are electrical conductors, the empty sites represent insulators, and that electrical current can flow only between nearest-neighbor conductor sites.

At low concentration p , the conductor sites are either isolated or form small clusters of nearest-neighbor sites. Two conductor sites belong to the same cluster if they are connected by a path of nearest-neighbor conductor sites, and a current can flow between them. At low p values, the mixture is an insulator, since no conducting path connecting opposite edges of our lattice exists. At large p values, on the other hand, many conduction paths between opposite edges exist, where electrical current can flow, and the mixture is a conductor.

At some concentration in between, therefore, a threshold concentration p_c must exist where for the first time electrical current can *percolate* from one edge to the other. Below p_c we have an insulator, above p_c we have a conductor. The threshold concentration is called the *percolation threshold*, or, since it separates two different phases, the *critical concentration*.

If the occupied sites are superconductors and the empty sites are conductors, p_c separates a normal-conducting phase below p_c from a superconducting phase

-
- ◀ **Fig. 2.0.** Site percolation clusters on a 510×510 square lattice, for $p=0.4, 0.5, 0.593, 0.65$. Different cluster sizes have different colors: empty sites are blue, clusters of one site are white. The color of the larger clusters depends on their size and varies from green (*small clusters*) via yellow and red to deep blue (infinite cluster at $p = 0.65$). Courtesy of S. Schwarzer

above p_c . Another example is a mixture of magnets and paramagnets, where the system changes at p_c from a paramagnet to a magnet.

In contrast to the more common thermal phase transitions, where the transition between two phases occurs at a critical temperature, the *percolation transition* described here is a *geometrical phase transition*, which is characterized by the geometric features of large clusters in the neighborhood of p_c . At low values of p only small clusters of occupied sites exist. When the concentration p is increased, the average size of the clusters increases. At the critical concentration p_c a large cluster appears which connects opposite edges of the lattice. We call this cluster the *infinite cluster*, since its size diverges when the size of the lattice is increased to infinity. When p is increased further, the density of the infinite cluster increases, since more and more sites become part of the infinite cluster. Accordingly, the average size of the *finite* clusters, which do not belong to the infinite cluster, decreases. At $p = 1$, trivially, all sites belong to the infinite cluster.

So far we have considered *site percolation*, where the sites of a lattice have been occupied randomly. When the bonds between the sites are randomly occupied, we speak of *bond percolation*. Two occupied bonds belong to the same cluster if they are connected by a path of occupied bonds (see Fig. 2.1). The critical concentration of bonds separates a phase of finite clusters of bonds from a phase with an infinite cluster.

Perhaps the most common example of bond percolation in physics is a *random resistor network*, where the metallic wires in a regular network are cut randomly with probability $q \equiv 1 - p$. Here q_c separates a conductive phase at low q from an insulating phase at large q .

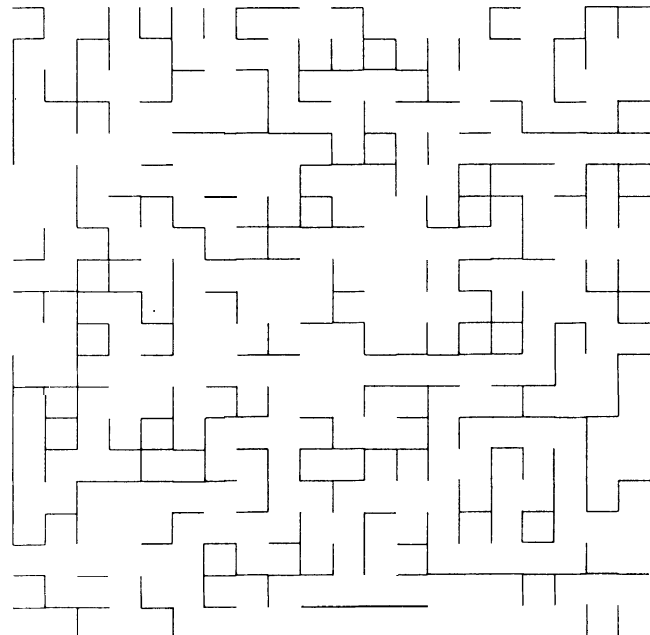


Fig. 2.1. Bond-percolation clusters on a 20×20 square lattice

A possible application of bond percolation in chemistry is the polymerization process [2.11–13], where small branching molecules can form large molecules by activating more and more bonds between them. If the activation probability p is above the critical concentration, a network of chemical bonds spanning the whole system can be formed, while below p_c only macromolecules of finite size can be generated. This process is called a *sole-gel* transition. An example of this *gelation* process is the boiling of an egg, which at room temperature is liquid and upon heating becomes a more solid-like *gel*.

An example from biology concerns the spreading of an epidemic [2.14]. In its simplest form, the epidemic starts with one sick individual, which can infect its nearest-neighbors with probability p in one time step. After one time step, it dies and the infected neighbors in turn can infect their (so far) uninfected neighbors, and the process is continued. Here the critical concentration separates a phase at low p where the epidemic always dies out after a finite number of time steps from a phase where the epidemic can continue forever. The same process can be used as a model for forest fires [2.1,15,83,87], with the infection probability replaced by the probability that a burning tree can ignite its nearest-neighbor trees in the next time step.

In addition to these simple examples, percolation aspects have been found useful to describe a large number of disordered systems in physics and chemistry [2.3,11,16–32], such as porous and amorphous materials [2.20] (including thin films [2.23]), disordered ionic conductors (including mixed-alkali glasses, two-phase mixtures [2.24], and dispersed ionic conductors [2.24–27]), branched polymers [2.28], fragmentation [2.29] (including nuclear fragmentation [2.30] and earthquakes [2.9,10]), galactic structures [2.31], and supercooled water [2.32].

The definitions of site and bond percolation on a square lattice can easily be generalized to any lattice in d dimensions. In general, in a given lattice, a bond has more nearest-neighbors than a site. For example, in the square lattice one bond is connected to six nearest-neighbor bonds, while a site has only four nearest-neighbor sites. Thus, large clusters of bonds can be formed more effectively than large clusters of sites, and a lower concentration of bonds is needed to form a spanning cluster; i.e., on a given lattice the percolation threshold for bonds is smaller than the percolation threshold for sites (see Table 2.1).

So far, we have focused on either site or bond percolation, where either sites *or* bonds of a given lattice have been chosen randomly. If sites are occupied with probability p *and* bonds are occupied with probability q , we speak of *site–bond percolation*. Two occupied sites belong to the same cluster if they are connected by a path of nearest-neighbor occupied sites with occupied bonds in between. For $q = 1$, site–bond percolation reduces to site percolation, for $p = 1$ it reduces to bond percolation. In general, both parameters characterize the state of the system. Accordingly, a *critical line* in p – q space separates both phases, which for $p = 1$ and $q = 1$ takes the values of the critical bond and site concentrations,

Table 2.1. Percolation thresholds for several two- and three-dimensional lattices and the Cayley tree (see Sect. 2.4.2). ^aExact [2.2,33,35]; ^bnumerical method [2.34]; ^cMonte-Carlo [2.1]; ^dseries expansion [2.36]; ^eMonte-Carlo [2.37]; ^fseries expansion [2.38]; ^gnumerical method [2.39]; ^hnumerical method [2.35]

Lattice	Percolation of sites bonds	
<i>Triangular</i>	$1/2^a$	$2 \sin(\pi/18)^a$
<i>Square</i>	$0.5927460^{b,h}$	$1/2^a$
<i>Honeycomb</i>	0.6962^c	$1-2\sin(\pi/18)^a$
<i>Face Centered Cubic</i>	0.198^c	0.119^c
<i>Body Centered Cubic</i>	0.245^c	0.1803^d
<i>Simple Cubic (1st nn)</i>	$0.31161^{e,g}$	0.248814^g
<i>Simple Cubic (2nd nn)</i>	0.137^f	—
<i>Simple Cubic (3rd nn)</i>	0.097^f	—
<i>Cayley Tree</i>	$1/(z-1)$	$1/(z-1)$

respectively. Site–bond percolations can be relevant for gelation and epidemic processes in dilute media (see Sect. 2.6).

The most natural example of percolation, perhaps, is *continuum percolation*, where the positions of the two components of a random mixture are not restricted to the discrete sites of a regular lattice. As a simple example, consider a sheet of conductive material, with circular holes punched randomly in it (Fig. 2.2). The relevant quantity now is the fraction p of remaining conductive material. Compared with site and bond percolation, the critical concentration is further decreased: $p_c \cong 0.312 \pm 0.005$ [2.40] for $d = 2$, when all circles have the same radius. This picture can easily be generalized to three dimensions, where spherical voids are generated randomly in a cube, and $p_c \cong 0.034 \pm 0.007$ [2.40,41]. Due to its similarity to Swiss cheese, this model of continuous percolation is called the Swiss cheese model. Similar models, where also the size of the spheres can vary, are used to describe sandstone and other porous materials.

Let us end this introductory section with some historical remarks. The first work introducing the concept of percolation was performed by Flory and Stockmayer about 50 years ago, when studying the gelation process [2.42]. The name percolation was suggested by Broadbent and Hammersley in 1957 when studying the spreading of fluids in random media [2.43]. They also introduced the relevant geometrical and probabilistic concepts. The developments of phase transition theory in the following years, in particular the series expansion method by Domb [2.5] and the renormalization group theory by Wilson, Fisher, and Kadanoff [2.44], stimulated tremendously the research activities on the geometric percolation transition. The fractal concepts introduced by Mandelbrot [2.45], have made available powerful new tools, which, together with the development of large-scale computers, have contributed significantly to our present understanding of percolation.

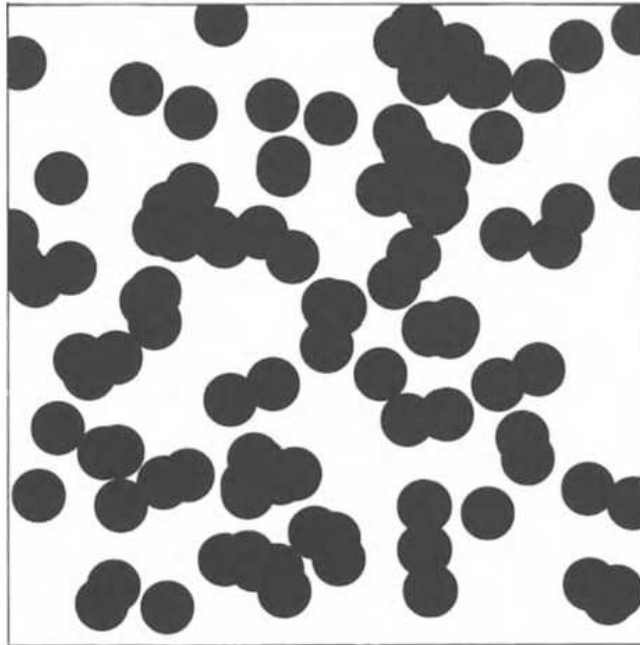


Fig. 2.2. Continuum percolation: Swiss cheese model

In this chapter we present mainly the static aspects of percolation, while dynamical properties associated with the percolation transition are discussed in Chap. 3.

2.2 Percolation as a Critical Phenomenon

The percolation transition is a simple example of a phase transition phenomenon. It is a geometrical phase transition where the critical concentration p_c separates a phase of finite clusters ($p < p_c$) from a phase where an infinite cluster is present ($p > p_c$). More common examples of phase transitions are thermal phase transitions such as the solid/liquid transition, where an ordered phase (the solid) changes into a disordered phase (the liquid) at some *critical* temperature T_c [2.46,47].

An illustrative example is the magnetic phase transition. At low temperatures some materials exhibit a spontaneous magnetization $m > 0$, without any external field (ferromagnetic phase). When the temperature increases the spontaneous magnetization decreases continuously and vanishes at the *critical* temperature T_c . Above T_c , in the paramagnetic phase, $m = 0$.

A magnetic material is composed of elementary magnetic moments (spins). The interactions between them favor an ordered state where all spins are parallel, while the thermal energy favors a disordered state where the spins have random orientation. At low temperatures, the interaction dominates and long-range order occurs, which is reflected by the nonzero spontaneous magneti-

zation m . Since m describes the order in the system, it is called the *order parameter*. With increasing temperature, $m(T)$ decreases and close to T_c follows a power law, $m(T) \sim (T_c - T)^\beta$. Above T_c , the thermal energy dominates, only finite clusters of temporarily aligned spins can exist, and their random orientation leads to zero magnetization.

In percolation, the concentration p of occupied sites plays the same role as the temperature in thermal phase transitions. We will see later that as with thermal transitions, long-range correlations control the percolation transition and the relevant quantities near p_c are described by power laws and critical exponents.

The percolation transition is characterized by the geometrical properties of the clusters near p_c . An important quantity is the probability P_∞ that a site (or a bond) belongs to the infinite cluster. For $p < p_c$, only finite clusters exist, and $P_\infty = 0$. For $p > p_c$, P_∞ behaves similarly to the magnetization below T_c , and increases with p by a power law

$$P_\infty \sim (p - p_c)^\beta. \quad (2.1)$$

Similarly to the magnetization, P_∞ describes the order in the percolation system and can be identified as the *order parameter*.

The linear size of the *finite* clusters, below and above p_c , is characterized by the *correlation length* ξ . The correlation length is defined as the mean distance between two sites on the same finite cluster. When p approaches p_c , ξ increases as

$$\xi \sim |p - p_c|^{-\nu}, \quad (2.2)$$

with the same exponent ν below and above the threshold. The mean number of sites (mass) of a finite cluster also diverges,

$$S \sim |p - p_c|^{-\gamma}, \quad (2.3)$$

again with the same exponent γ above and below p_c . To obtain ξ and S , averages over all finite clusters in the lattice are required.

Analogs of the quantities P_∞ and S in magnetic systems are the magnetization m and the susceptibility χ (see Fig. 2.3 and Table 2.2).

The exponents β , ν , and γ describe the critical behavior of typical quantities associated with the percolation transition, and are called the *critical exponents*. The exponents are universal and depend neither on the structural details of the lattice (e.g., square or triangular) nor on the type of percolation (site, bond, or continuum), but only on the dimension d of the lattice.

This universality property is a general feature of phase transitions, where the order parameter vanishes continuously at the critical point (second-order phase transition). For example, the magnetization in all three-dimensional magnetic materials is described by the same exponent β , irrespective of the crystalline structure or the type of interactions between the spins, as long as they are of short range.

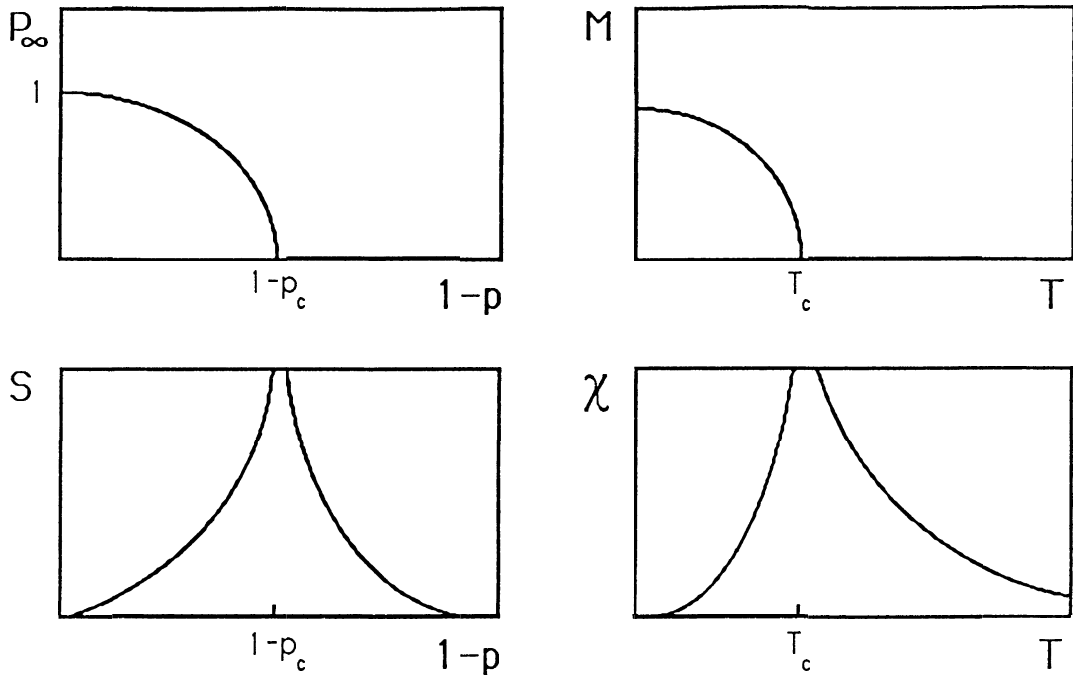


Fig. 2.3. P_∞ and S compared with magnetization m and susceptibility χ

The exponents β , ν , and γ are not the only critical exponents characterizing the percolation transition. The size distribution of percolation clusters, for example, is described by other exponents α , τ , and σ . However, as we show in Sect. 2.5 there exist relations between these exponents, and all of them can be obtained from the knowledge of just two of them.

In Table 2.2, the values of the critical exponents β , ν , and γ in percolation are listed for two, three, and six dimensions. They are compared with the analogous exponents of the magnetic phase transition.

The exponents considered here describe the geometrical properties of the percolation transition. The physical properties associated with the transition also show power-law behavior near p_c and are characterized by critical exponents.

Table 2.2. Exact values and best estimates for the critical exponents in percolation and magnetism. ^aExact [2.48,49]; ^bnumerical simulations [2.37]; ^cexact [2.4,6]

Percolation	$d=2$	$d=3$	$d \geq 6$
<i>Order parameter</i> P_∞ : β	$5/36^a$	0.417 ± 0.003^b	1^c
<i>Correlation length</i> ξ : ν	$4/3^a$	0.875 ± 0.008^b	$1/2^c$
<i>Mean cluster size</i> S : γ	$43/18^a$	1.795 ± 0.005^b	1^c
Magnetism	$d=2$	$d=3$	$d \geq 6$
<i>Order parameter</i> m : β	$1/8$	0.32	$1/2$
<i>Correlation length</i> ξ : ν	1	0.63	$1/2$
<i>Susceptibility</i> χ : γ	$7/4$	1.24	1

Examples are the conductivity in a random resistor or random superconducting network, or the spreading velocity of an epidemic disease near the critical infection probability. Presumably their “dynamical” exponents cannot be generally related to the geometric exponents discussed above. A review on the transport properties of percolation is given in Chap. 3.

At the end of this section we note that all quantities described above are defined in the thermodynamic limit of large systems. In a finite system, P_∞ , for example, is not strictly zero below p_c . An approach to finite-size effects will be discussed in Sect. 2.5.

2.3 Structural Properties

a) The fractal dimension d_f . As was first noticed by Stanley [2.51], the structure of percolation clusters can be well described by the fractal concept [2.45]. We begin by considering the infinite cluster at the critical concentration p_c . A representative example of the infinite cluster is shown in Fig. 2.4.

As seen in the figure, the infinite cluster contains holes of all sizes, similarly to the Sierpinski gasket (see Chap. 1 and Sect. 2.8). The cluster is self-similar on all length scales (larger than the unit size and smaller than the lattice size), and can be regarded as a fractal. The fractal dimension d_f describes how, on average, the mass M of the cluster within a sphere of radius r scales with r ,

$$M(r) \sim r^{d_f}. \quad (2.4)$$

As explained in Chap. 1, in random fractals $M(r)$ represents an average over many different cluster configurations or, equivalently, over many different centers of spheres on the same infinite cluster.

Below and above p_c , the mean size of the *finite* clusters in the system is described by the correlation length ξ . At p_c , ξ diverges and holes occur in the infinite cluster on all length scales. Above p_c , ξ also represents the linear size of the holes in the infinite cluster. Since ξ is finite above p_c , the infinite cluster can be self-similar only on length scales smaller than ξ . We can interpret $\xi(p)$ as a typical length up to which the cluster is self-similar and can be regarded as a fractal. For length scales larger than ξ , the structure is not self-similar and can be regarded as homogeneous. The crossover from the fractal behavior at small length scales to a homogeneous behavior at large length scales is best illustrated by a lattice composed of Sierpinski gasket unit cells of size ξ (see Fig. 2.5).

If our length scale is smaller than ξ , we see a fractal structure. On length scales larger than ξ , we see a homogeneous system which is composed of many unit cells of size ξ . Mathematically, this can be summarized as

$$M(r) \sim \begin{cases} r^{d_f}, & r \ll \xi, \\ r^d, & r \gg \xi. \end{cases} \quad (2.5)$$

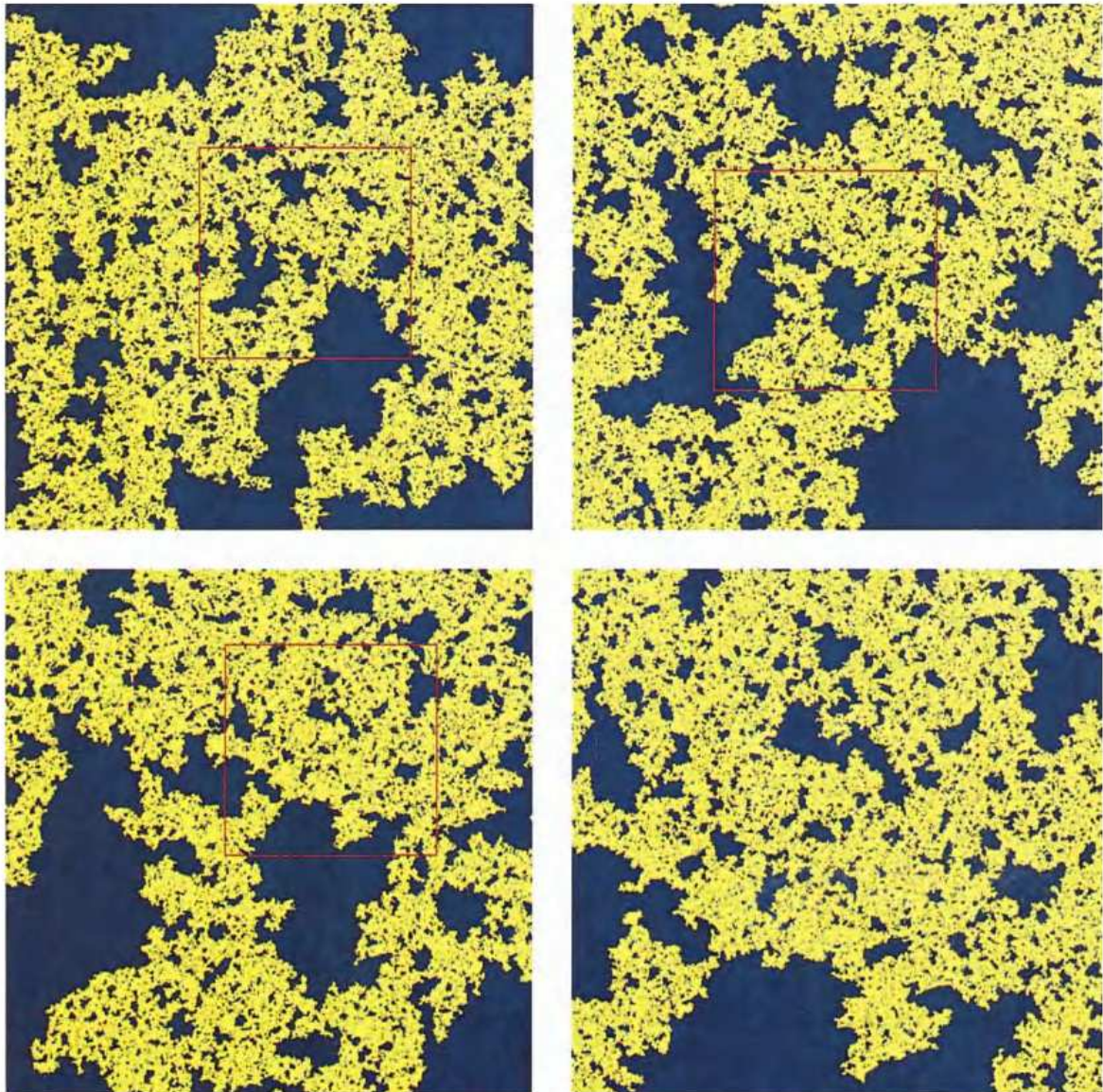


Fig. 2.4. Self-similarity of a large percolation cluster at the critical concentration. The cluster was grown by the Leath method (see Sect. 2.7.2) and consists of 20 000 shells. Courtesy of M. Meyer

Figure 2.6 shows this crossover in a $2d$ percolation system for p above p_c . One can relate the fractal dimension d_f of percolation clusters to the exponents β and ν . The probability that an arbitrary site within a circle of radius r smaller than ξ belongs to the infinite cluster, is the ratio between the number of sites on the infinite cluster and the total number of sites,

$$P_\infty \sim \frac{r^{d_f}}{r^d}, \quad r < \xi. \quad (2.6)$$

This equation is certainly correct for $r = a\xi$, where a is an arbitrary constant smaller than 1. Substituting $r = a\xi$ in (2.6) yields

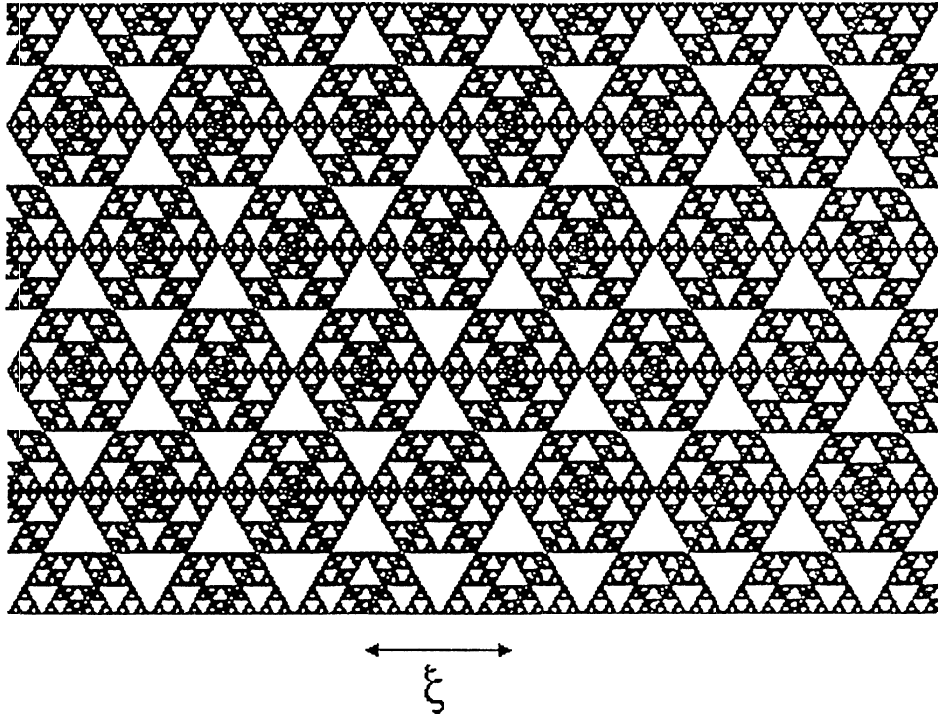


Fig. 2.5. Lattice composed of Sierpinski gasket cells of size ξ

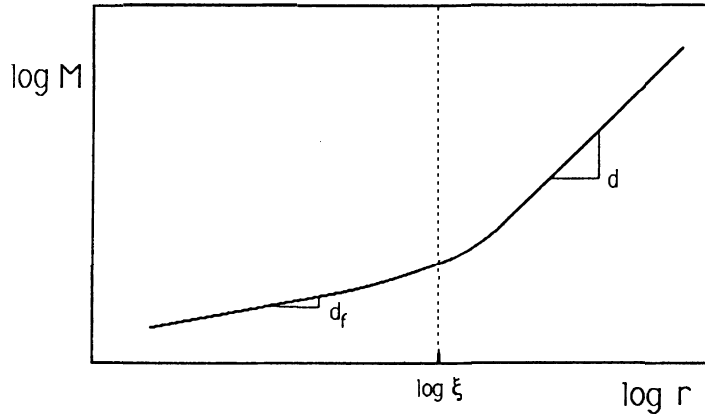


Fig. 2.6. Schematic plot of the crossover of $M(r)$ above the percolation threshold. For $r \ll \xi$ the slope is d_f while for $r \gg \xi$ the slope is d

$$P_\infty \sim \frac{\xi^{d_f}}{\xi^d}. \quad (2.7)$$

Both sides are powers of $p - p_c$. Substituting (2.1) and (2.2) into (2.7) we obtain [2.4, 40, 41],

$$d_f = d - \frac{\beta}{\nu}. \quad (2.8)$$

Thus the fractal dimension of the infinite cluster at p_c is not a new independent exponent but depends on β and ν . Since β and ν are universal exponents, d_f

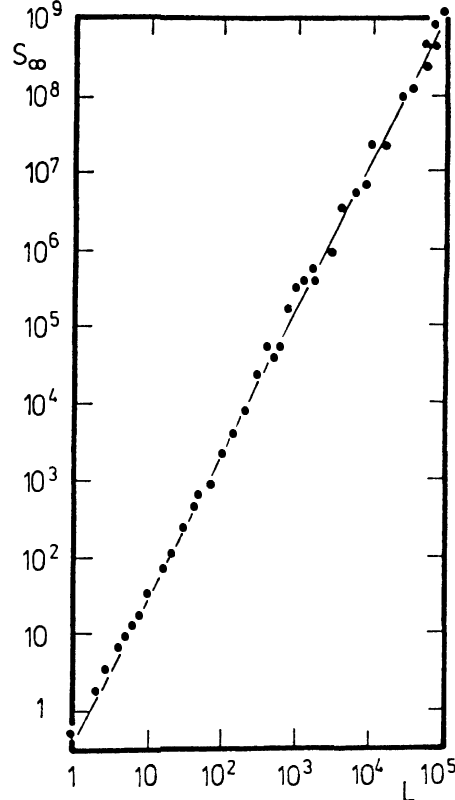


Fig. 2.7. The size of the largest cluster at the critical concentration $p_c = 1/2$ of the triangular lattice as a function of the linear size L of the lattice. For large L , the slope of this log-log plot is very close to the predicted value $d_f = 91/48$. (After [2.1])

is also universal. The actual dependence of $M(L)$ on the system linear size L for site percolation on a triangular lattice is shown in Fig. 2.7 [2.1]. At large values of L , the curve in the double logarithmic plot approaches a straight line with slope $d_f \cong 91/48$, in agreement with (2.8).

It can be shown that (2.8) also represents the fractal dimension of the finite clusters at p_c and below p_c , as long as their linear size is smaller than ξ . Below p_c there also exist (though very rarely) clusters with a linear size larger than ξ . These clusters are called *lattice animals* and their fractal dimension is smaller than d_f [2.53,54].

b) The graph dimensions d_{\min} and d_ℓ . The fractal dimension, however, is not sufficient to fully characterize a percolation cluster. This becomes evident for example, on comparing pictures of diffusion limited aggregates (DLA) (see Chaps. 1, 4 and 10) and percolation clusters. The two clusters look very different. The percolation cluster has loops on all length scales, while the aggregate has practically no loops. In $d = 3$, both structures retain their characteristic differences, but their fractal dimensions are nearly the same, $d_f \cong 2.5$.

For a further intrinsic characterization of a fractal we consider the shortest path between two arbitrary sites A and B on the cluster (see Figs. 2.8–10) [2.14,55–59]. The structure formed by the sites of this path is also self-similar

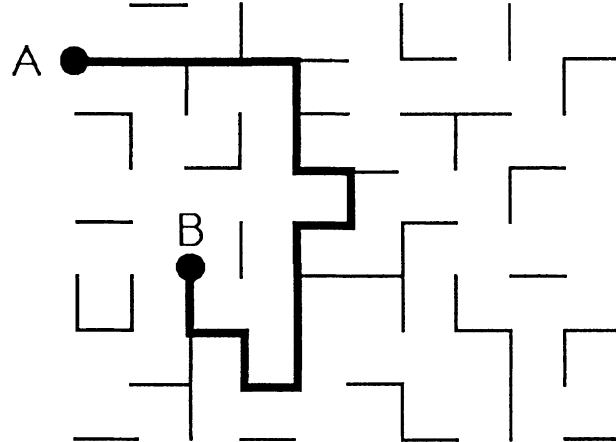


Fig. 2.8. Shortest path between two sites A and B on a percolation cluster

and is described by a fractal dimension d_{\min} [2.60,61]. Accordingly, the length ℓ of the path, which is often called the “chemical distance”, scales with the “Euclidean distance” r between A and B as

$$\ell \sim r^{d_{\min}}. \quad (2.9a)$$

The inverse relation

$$r \sim \ell^{1/d_{\min}} \equiv \ell^{\bar{\nu}} \quad (2.9b)$$

tells how r scales with ℓ .

Closely related to d_{\min} and d_f is the “chemical” dimension d_ℓ , which describes how the cluster mass M within the chemical distance ℓ from a given site scales with ℓ ,

$$M(\ell) \sim \ell^{d_\ell}. \quad (2.10)$$

While the fractal dimension d_f characterizes how the mass of the cluster scales with the “Euclidean” distance r , the graph dimension d_ℓ characterizes how the mass scales with the chemical distance ℓ . The different arrangement of the cluster sites in ℓ and r space is demonstrated in Fig. 3.0. Combining (2.4), (2.9a), and (2.10) we obtain the relation between d_{\min} , d_ℓ , and d_f

$$d_\ell = \frac{d_f}{d_{\min}}. \quad (2.11)$$

To measure d_f , an arbitrary site is chosen on the cluster and one determines the number $M(r)$ of all sites within a distance r from this site. To measure d_ℓ , an arbitrary site is chosen on the cluster and one determines the number $M(\ell)$ of all sites which are connected to this site by a shortest path with length smaller or equal to ℓ . Finally, to measure d_{\min} , two arbitrary sites at Euclidean distance r are chosen on the cluster and one determines the length $\ell(r)$ of the shortest path connecting them. As for $M(r)$, averages have to be performed for $M(\ell)$ and $\ell(r)$ over many realizations. In regular “Euclidean” lattices, both d_ℓ and d_f coincide with the Euclidean space dimension d and $d_{\min} = 1$.

The chemical dimension d_ℓ (or $d_{\min} = 1/\tilde{\nu}$) is an important tool for distinguishing between different fractal structures which may have a similar fractal dimension. In $d = 3$ for example, DLA clusters and percolation clusters have approximately the same fractal dimension $d_f \cong 2.5$, but have different $\tilde{\nu}$: $\tilde{\nu} = 1$ for DLA [2.62] but $\tilde{\nu} \cong 0.73$ for percolation [2.39,72,75,77].

While d_f has been related to the (known) critical exponents, (2.8), no such relation has been found (yet) for d_{\min} or d_ℓ . The values of d_ℓ or d_{\min} are known only from approximate methods, mainly numerical simulations.

The concept of the chemical distance also plays an important role in the description of dynamic phenomena in disordered systems, such as the spreading of forest fires or epidemics, that propagate along the shortest path from the seed. In Sect. 2.6 it is shown that the velocity with which the fire front or the epidemic propagates is related to the exponent $\tilde{\nu}$. Other examples where the concept of the chemical distance is essential include the diffusion of particles and localized vibrational excitation (see Sects. 3.2 and 3.7).

c) Probability densities. The relations between M , r , and ℓ are fully characterized by the probability densities $\phi(M | r)$, $\phi(M | \ell)$, and $\phi(r | \ell)$ [2.63,65]. $\phi(M | r)$ is the probability that within a circle of radius r there exist M cluster sites. Accordingly, $\phi(M | \ell)$ is the probability of finding M cluster sites within ℓ chemical shells, and $\phi(r | \ell)$ is the probability that two cluster sites separated by chemical distance ℓ are at (Euclidean) distance r from each other. The mean quantities $M(r)$, $M(\ell)$, and $r(\ell)$ discussed in (2.4), (2.9), and (2.10) represent the *first moments* of these distributions, e.g., $M(r) = \int M' \phi(M' | r) dM'$.

It is expected that the probability densities scale as [2.63] (see also Sect. 2.5)

$$\phi(M | r) \sim \frac{1}{M} f \left(\frac{M}{r^{d_f}} \right). \quad (2.12)$$

Of particular importance for the dynamical properties of percolation clusters (see Sects. 3.2 and 3.7) are the probability density $\phi(\ell | r)$, which is the probability that two cluster sites at an Euclidean distance r are separated by the chemical distance ℓ , and the analogous quantity $\phi(r | \ell)$.

Numerically, $\phi(r | \ell)$ can be obtained as follows. First one chooses one cluster site as a center site and counts the number $N(\ell)$ of all sites that are at a given chemical distance ℓ from this site. Among these $N(\ell)$ sites, there are $N(r, \ell)$ sites at an Euclidean distance r from the center (see Fig. 2.9). The fraction $N(r, \ell)/N(\ell)$, averaged over many configurations, can be identified with $\phi(r | \ell)$. The related probability density $\phi(\ell | r)$ is obtained in a similar way by calculating the number of sites $N(r)$ that are at an Euclidean distance r from the center, and averaging over the fraction $N(r, \ell)/N(r)$. Since by definition $\sum_r N(r, \ell) = N(\ell)$ and $\sum_\ell N(r, \ell) = N(r)$, the probability densities satisfy, in the continuum limit, the normalization condition $\int \phi(r | \ell) dr = \int \phi(\ell | r) d\ell = 1$.

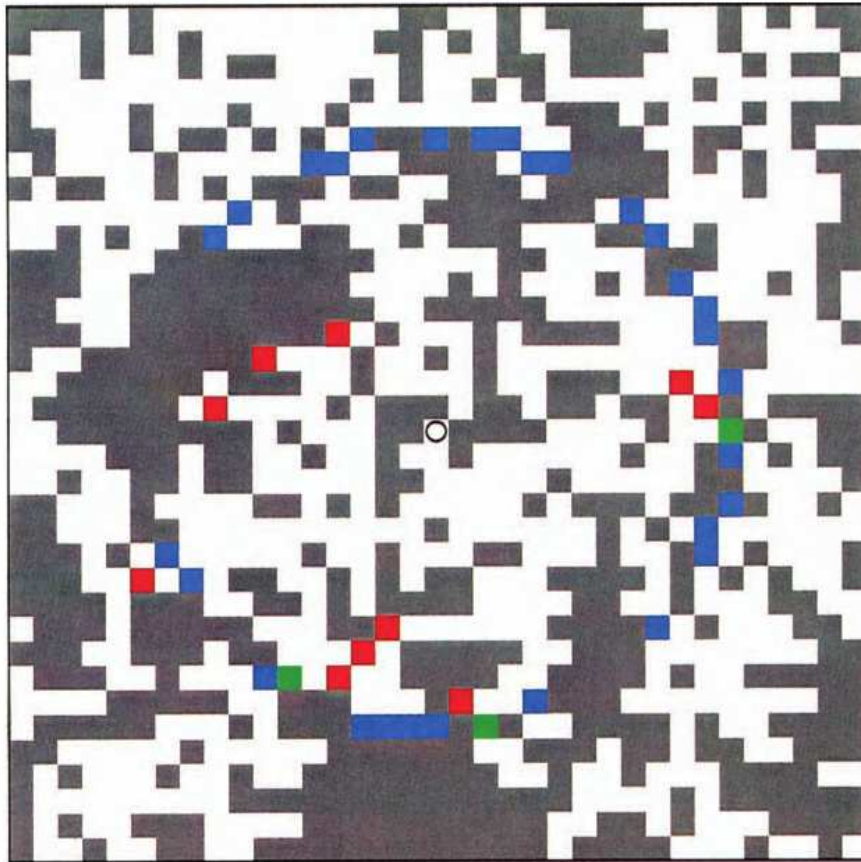


Fig. 2.9. A percolation cluster at the critical concentration in a square lattice. The sites located between $r = 9.5$ and 10.5 from the center site (\circ) are in blue, the sites located between $\ell = 14.5$ and 15.5 from the center site are in red, and those sites that are between $r = 9.5$ and 10.5 and between $\ell = 14.5$ and 15.5 are in red. Courtesy of J. Dräger and M. Meyer

Since $N(\ell)$ and $N(r)$ scale as

$$N(\ell) \sim \ell^{d_\ell - 1}, \quad N(r) \sim r^{d_f - 1}, \quad (2.13)$$

both probability densities are related by

$$\phi(\ell \mid r) \propto \phi(r \mid \ell) \ell^{d_\ell - 1} / r^{d_f - 1}. \quad (2.14)$$

For a percolation cluster, $\phi(r \mid \ell)$ cannot be calculated analytically. To obtain an idea about the specific functional form of $\phi(r \mid \ell)$, let us first consider a much simpler random fractal structure: the trace of a random walker in a high-dimensional lattice ($d \geq 4$) (see Chap. 1 and Sect. 3.2 with Fig. 3.3). For ($d \geq 4$), intersections of the trace are very rare, and the structure can be considered as linear ($d_\ell = 1$). By construction, the length ℓ of this random-walk chain is identical to the number of steps t performed by the random walker. Hence, $\phi(r \mid \ell)$ for the random-walk chain has the same form as the well-known probability $P(r, t)$ of finding the random walker at time step t a distance r from his starting point, i.e., (see Sect. 3.2)

$$\phi(r \mid \ell) \propto \ell^{-d/2} \exp(-dr^2/2\ell). \quad (2.15)$$

There is numerical evidence [2.63] that a similar functional form holds also for percolation clusters,

$$\phi(r \mid \ell) = (C_1/r)(r/\ell^{\tilde{\nu}})^{g+d_f} \exp[-C_2(r/\ell^{\tilde{\nu}})^{\tilde{\delta}}], \quad \tilde{\delta} = (1 - \tilde{\nu})^{-1}, \quad (2.16)$$

where C_1 and C_2 are (nonuniversal) constants and g is a new exponent, $g \approx 1.32$ ($d = 2$) and $g \approx 1.5$ ($d = 3$) [2.63, 64]. For $d = d_c = 6$ it is expected that $g = 2$ [2.65]. For very small values of $r/\ell^{\tilde{\nu}}$, the values of g tend to be smaller [2.65]. Similar scaling forms also hold for $\phi(M \mid \ell)$ and $\phi(M \mid r)$.

It is obvious, however, that for fixed r , (2.15,16) do not hold for arbitrary small ℓ -values, since there exists a minimum chemical distance $\ell_{\min}(r)$ that a cluster site at Euclidean distance r from the center site can have. This quantity plays an important role when transport and vibrational properties of percolation clusters are studied. In contrast to the other quantities discussed in this chapter, $\ell_{\min}(r)$ is not self-averaging, but depends (logarithmically) on the number N of configurations averaged [2.64],

$$\ell_{\min}(r) \equiv \ell_{\min}(r, N) = \begin{cases} r, & r \ll r_c(N), \\ r_c(N)^{1-d_{\min}} r^{d_{\min}}, & r \gg r_c(N), \end{cases} \quad (2.17)$$

where the “crossover” length $r_c(N)$ is given by $r_c(N) = (\ln z + \ln N)/\ln(1/p_c)$, and z is the coordination number of the underlying lattice; $z = 4$ for the square and $z = 6$ for the simple cubic lattice.

d) Fractal substructures. Next we show that d_f and d_ℓ are not the only exponents characterizing a percolation cluster at p_c . As is illustrated in Fig. 2.10, a percolation cluster is composed of several fractal substructures, which are described by other exponents. Imagine applying a voltage difference between two sites at opposite edges of a metallic percolation cluster: The *backbone* of the cluster consists of those sites (or bonds) which carry the electric current. The *dangling ends* are those parts of the cluster which carry no current and are connected to the backbone by a single site only. The *red bonds* (or singly connected bonds) [2.51, 66] are those bonds that carry the total current; when they are cut the current flow stops. In analogy to red bonds we can define anti-red bonds [2.67]. If an anti-red bond is added to a nonconducting percolation system below p_c , the current will be able to flow in the system. The *blobs*, finally, are those parts of the backbone that remain after the red bonds have been removed.

Further substructures of the cluster are the *external perimeter* (which is also called the *hull*), the *skeleton*, and the *elastic backbone*. The hull consists of those sites of the cluster which are adjacent to empty sites and are connected with infinity via empty sites. In contrast, the *total perimeter* also includes the holes in the cluster. The external perimeter is an important model for random fractal interfaces (see Chaps. 7 and 8). The skeleton is defined as the union of

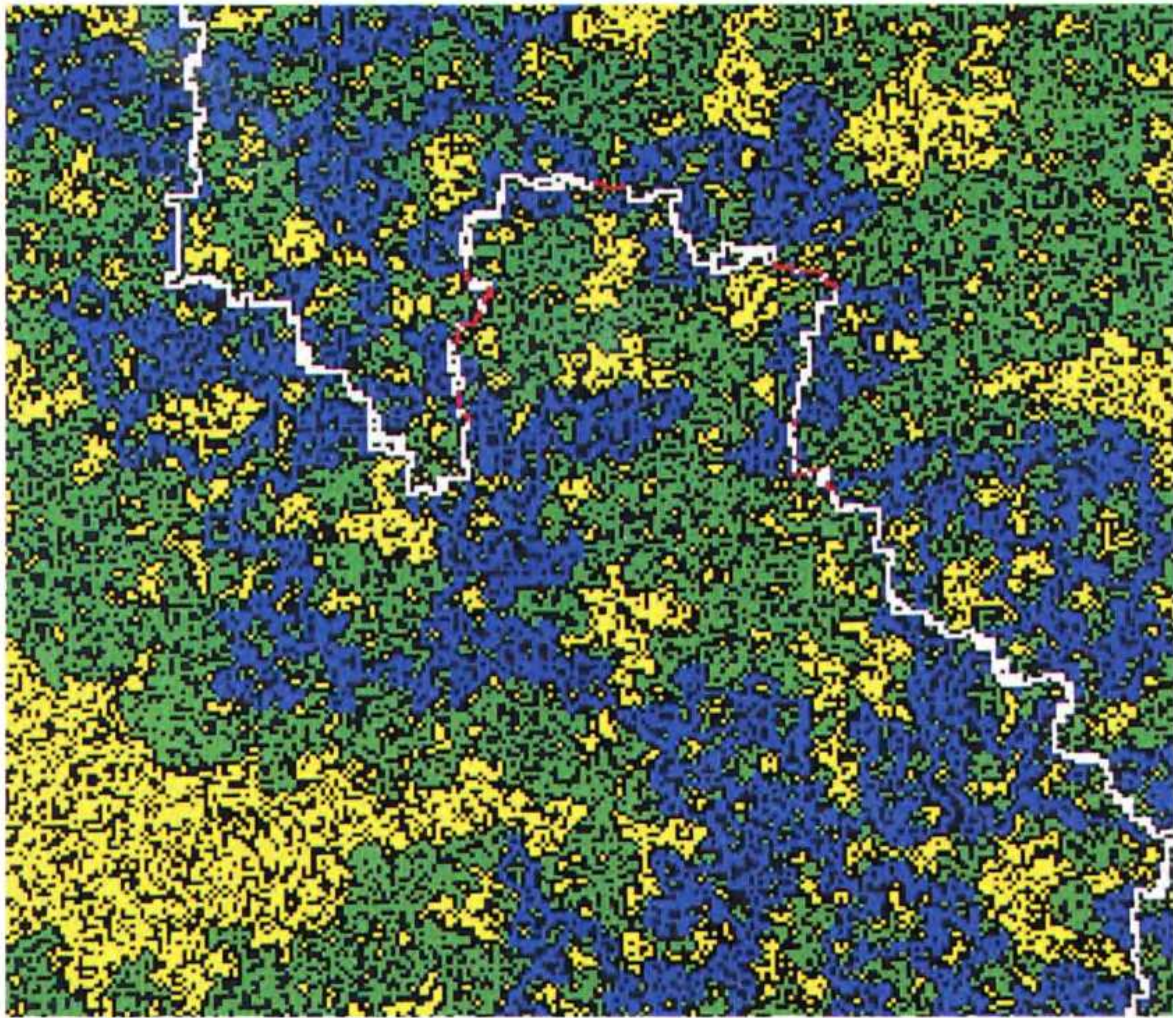


Fig. 2.10. Percolation system at the critical concentration in a 510×510 square lattice. The finite clusters are in yellow. The substructures of the infinite percolation cluster are shown in different colors: the shortest path between two points at opposite sites of the system is shown in white, the single connected sites (“red” sites) in red, the loops in blue, and the dangling ends in green. Courtesy of S. Schwarzer

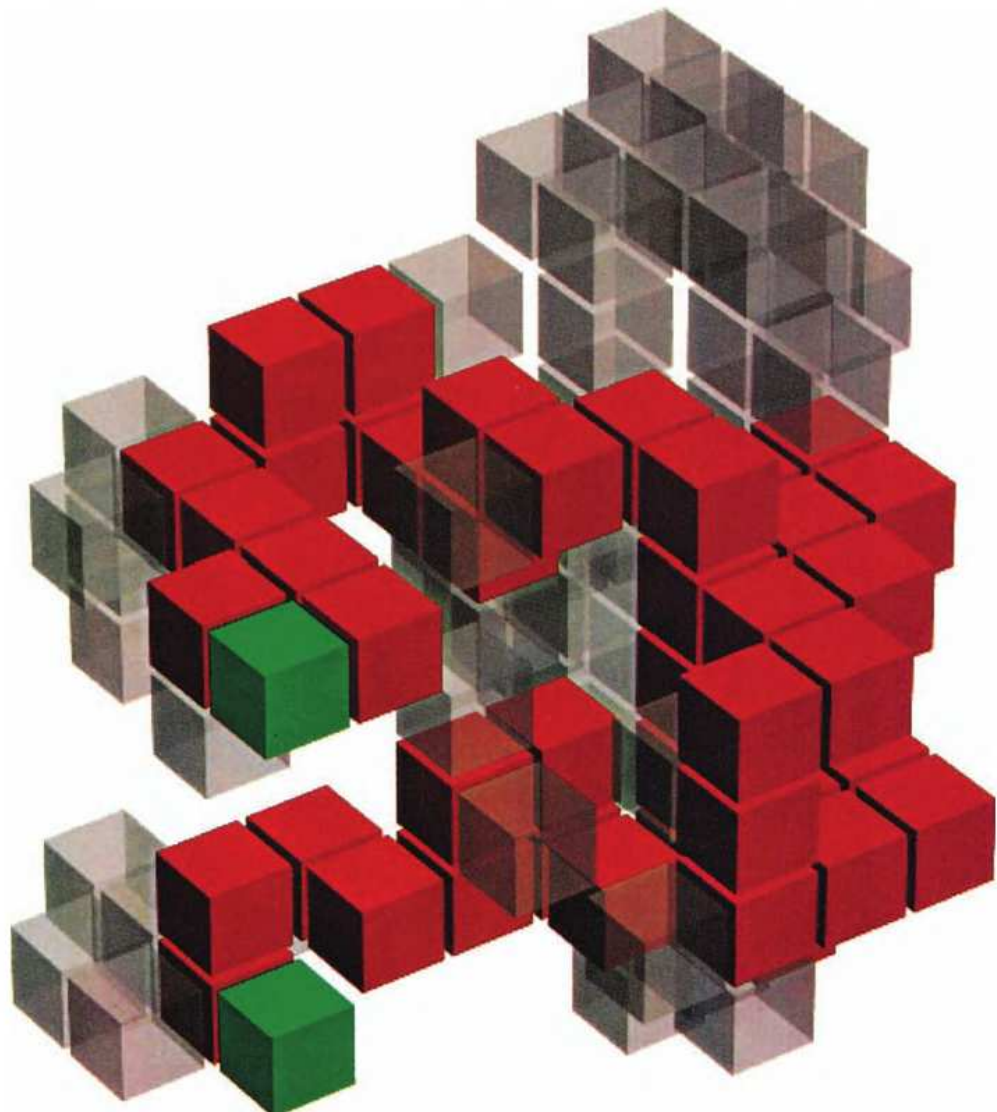
all shortest paths from a given site to all sites at a chemical distance ℓ [2.68]. The elastic backbone is the union of all shortest paths between two sites [2.69].

The fractal dimension d_B of the backbone is smaller than the fractal dimension d_f of the cluster (see Table 2.3). This reflects the fact that most of the mass of the cluster is concentrated in the dangling ends, which is seen clearly in Fig. 2.11. The value of the fractal dimension of the backbone is known only from numerical simulations [2.70]. A recent conjecture yields $d_B = 13/8$ [2.75].

Fig. 2.11. Percolation cluster at the critical concentration in a simple cubic lattice. The backbone between two (green) cluster sites is shown in red, the gray sites represent the dangling ends. Courtesy of M. Porto

Table 2.3. Fractal dimensions of the substructures composing percolation clusters. Exact results and best estimates are presented: ^aexact [2.48,49]; ^bnumerical simulations [2.37]; ^cnumerical simulations [2.61,63]; ^dnumerical simulations [2.70a]; ^eexact [2.66,71]; ^fexact [2.72,73]; ^gnumerical simulations [2.37]; ^hnumerical simulations [2.39]; ⁱnumerical simulations [2.84]; ^knumerical simulations [2.70b]. For other estimates see Sects. 2.7 and 2.8

Fractal dimensions	Space dimension		
	d=2	d=3	d ≥ 6
d_f	91/48 ^a	2.524 ± 0.008^b	4
d_ℓ	1.678 ± 0.005^c	1.84 ± 0.02^i	2
d_{\min}	1.13 ± 0.004^c	1.374 ± 0.004^h	2
d_{red}	$3/4^e$	1.143 ± 0.01^b	2
d_h	$7/4^f$	2.548 ± 0.014^g	4
d_B	1.62 ± 0.02^d	1.855 ± 0.015^k	2
d_ℓ^B	1.45 ± 0.02^i	1.37 ± 0.03^i	1



Note that also the graph dimension d_ℓ^B of the backbone is smaller than that of percolation. In contrast, $\tilde{\nu}$ is the *same* for both the percolation cluster and its backbone, indicating the more universal nature of $\tilde{\nu}$. This can be understood since every two sites on a percolation cluster can be located on the corresponding backbone.

The fractal dimensions of the red bonds d_{red} and the hull d_h are known from exact analytical arguments. It has been proven by Coniglio [2.66,71] (see Sect. 2.8) that the mean number of red bonds varies with p as

$$n_{\text{red}} \sim (p - p_c)^{-1} \sim \xi^{1/\nu} \sim r^{1/\nu}, \quad (2.18)$$

and the fractal dimension of the red bonds is therefore $d_{\text{red}} = 1/\nu$. The fractal dimension of the skeleton is very close to $d_{\text{min}} = 1/\nu$, supporting the assumption that percolation clusters at criticality are finitely ramified [2.68] (see Sect. 2.8).

The hull of the cluster in $d = 2$ has the fractal dimension $d_h = 7/4$, which was first found numerically by Sapoval, Rosso, and Gouyet [2.72] and proven rigorously by Saleur and Duplantier [2.73]. If the hull is defined slightly differently and next-nearest neighbors of the perimeter are regarded as connected, many “fjords” are removed from the hull. According to Grossmann and Aharony [2.74], the fractal dimension of this modified hull is close to $4/3$, the fractal dimension of self-avoiding random walks. In three dimensions, in contrast, the mass of the hull seems to be proportional to the mass of the cluster, and both have the same fractal dimension (see also Chap. 7).

In Table 2.3 the values of the fractal dimension d_f and the graph dimension d_ℓ of the percolation cluster and its fractal substructures are summarized. The values for six dimensions are known rigorously from considerations given in the following sections.

2.4 Exact Results

Only very few results for the percolation problem can be obtained exactly. Some special cases can be treated exactly [2.1,2,6] and will be discussed here. From these examples, one easily becomes acquainted with the common definitions, techniques, and concepts used in percolation theory.

2.4.1 One-Dimensional Systems

Consider a one-dimensional chain, where each site is occupied randomly with probability p . Clusters are groups of neighboring sites. The sites neighboring the left and right end sites of a cluster must be empty. Since an infinite cluster can occur only if *all* sites in the chain are occupied, it follows that $p_c = 1$. Thus, only quantities below p_c , such as the correlation length or the mean number of sites (mass) of a cluster, can be calculated here.

We begin with the correlation length ξ and the correlation function $g(r)$, which is the mean number of sites on the same cluster at distance r from an arbitrary occupied site. In order for two sites separated a distance r to belong to the same cluster, all $r - 1$ sites in between must be occupied. Since the occupation is a random process with probability p ,

$$g(r) = 2p^r. \quad (2.19)$$

The factor 2 comes from the fact that the site can be either to the left or to the right of the origin. The correlation length ξ is defined as the mean distance between two sites on the same cluster,

$$\xi^2 = \frac{\sum_{r=1}^{\infty} r^2 g(r)}{\sum_{r=1}^{\infty} g(r)} = \frac{\sum_{r=1}^{\infty} r^2 p^r}{\sum_{r=1}^{\infty} p^r}. \quad (2.20)$$

The sums can be performed easily and one obtains

$$\xi^2 = \frac{1+p}{(1-p)^2} \equiv \frac{1+p}{(p_c - p)^2}. \quad (2.21)$$

Thus we find $\nu = 1$ in one dimension. Using this result, one can express the correlation function $g(r)$ near p_c by an exponential:

$$\ln g(r) \sim -r/\xi, \quad (2.22)$$

where the correlation length ξ represents the decay radius of the correlation function.

Next we consider the mean mass S of the finite clusters. The mean mass S can be written as

$$S = 1 + \sum_{r=1}^{\infty} g(r), \quad (2.23)$$

where the 1 comes from the site at the origin, which was assumed to be occupied. From (2.23) it follows that

$$S = \frac{1+p}{1-p} \sim (p_c - p)^{-1}, \quad (2.24)$$

and hence $\gamma = 1$ in one dimension.

A quantity which plays a central role in the description of the cluster statistics is the probability that a chosen lattice site belongs to a cluster of s sites. This probability is given by $sp^s(1-p)^2$. The factor s is due to the fact that the chosen site can be any of the s sites in the cluster. The factor $(1-p)^2$ is due to the fact that every cluster must be surrounded by perimeter sites which are empty. In $d = 1$, every cluster has two perimeter sites. It is convenient to define the corresponding probability per cluster site, n_s , which in this case is

$$n_s = p^s(1-p)^2. \quad (2.25)$$

This quantity can also be interpreted as the number of clusters of size s divided by the total number of sites in the system. By definition, $\sum_{s=1}^{\infty} s n_s = p$, which can be easily checked using (2.25). The mean cluster mass S is related to n_s by

$$S = \sum_{s=1}^{\infty} s \left(\frac{s n_s}{\sum_{s=1}^{\infty} s n_s} \right). \quad (2.26)$$

Here the factor $(s n_s / \sum s n_s)$ is the probability that an occupied site belongs to a cluster of s sites. The sum in (2.26) can be performed easily, and of course gives the same result as (2.24).

The drawback of the one-dimensional chain is that there is no concentration range above p_c and thus the critical properties above p_c cannot be studied. Below p_c , however, the system shows critical (power-law) behavior, similar to the behavior in higher dimensions.

2.4.2 The Cayley Tree

A second system in which the percolation problem can be solved rigorously is the Cayley tree (also called the Bethe lattice) [2.1,6,62]. The Cayley tree has the advantage that the critical concentration is smaller than 1 and the regime above p_c can also be studied.

The Cayley tree is a structure without loops which is generated as follows. We start with a central site from which z branches (of unit length) emanate. The end of each branch is another site, and we obtain z sites which constitute the first shell of the Cayley tree. From each site $z - 1$ new branches grow out, generating $z(z - 1)$ sites in the second shell. This process is continued (see Fig. 2.12) and an infinite Cayley tree with z branches emanating from each site is generated. For $z = 2$, the tree reduces to the one-dimensional chain.

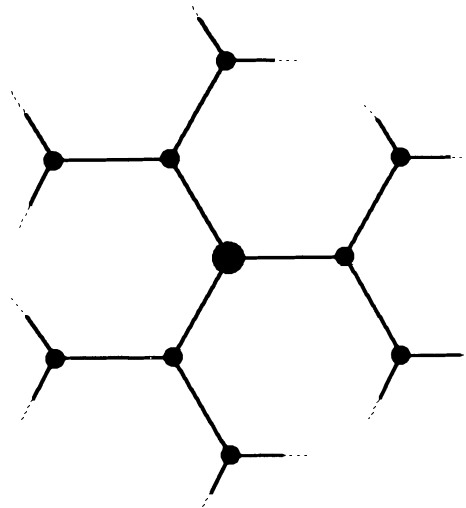


Fig. 2.12. Two shells of a Cayley tree, with $z = 3$

There are no loops in the system, since any two sites are connected by *only one* path. The Euclidean distance r has no meaning here, the lattice being described solely by the chemical distance ℓ between two sites. For example, the chemical distance between the central site and a site on the ℓ th shell is exactly ℓ .

The ℓ th shell of the tree consists of $z(z - 1)^{\ell-1}$ sites, increasing exponentially with ℓ . In a d -dimensional Euclidean lattice, with d finite, the number of sites at distance ℓ increases as ℓ^{d-1} . Since the exponential dependence can be considered as a power-law behavior with an infinite exponent, the Cayley tree can be regarded as an infinite-dimensional lattice. From the universality property we can expect that the critical exponents derived for percolation on the Cayley tree will be the same as for percolation on *any* infinite-dimensional lattice. Moreover, as will be shown below, the upper critical dimension for percolation is $d_c = 6$ [2.77–79], i.e., the critical exponents are the same for all dimensions $d \geq 6$. Thus we expect that the exponents for percolation on the Cayley tree are the same as in $d \geq 6$ dimensions.

As for the one-dimensional case, we begin with the correlation function $g(\ell)$, which is defined as the mean number of sites on the same cluster at distance ℓ from an arbitrary occupied site. In order that two sites separated a distance ℓ belong to the same cluster, all $\ell - 1$ sites in between must be occupied. Since the occupation is a random process with probability p , and each shell contains $z(z - 1)^{\ell-1}$ sites, it follows that

$$g(\ell) = z(z - 1)^{\ell-1} p^\ell \equiv \frac{z}{z - 1} [(z - 1)p]^\ell. \quad (2.27)$$

For $z = 2$, the Cayley tree reduces to a linear chain and (2.27) reduces to (2.19). From (2.27) the critical concentration p_c can be easily derived. For ℓ approaching infinity, the correlation function tends to zero exponentially for $p(z - 1) < 1$, and diverges for $p(z - 1) > 1$. Accordingly, an infinite cluster can be generated only if $p \geq 1/(z - 1)$. Hence

$$p_c = \frac{1}{z - 1} \quad (2.28)$$

for the Cayley tree. From (2.27) we can easily calculate the correlation length ξ_ℓ in ℓ space,

$$\xi_\ell^2 = \frac{\sum_{\ell=1}^{\infty} \ell^2 g(\ell)}{\sum_{\ell=1}^{\infty} g(\ell)}. \quad (2.29)$$

As for the linear chain, the sums can be performed easily to give

$$\xi_\ell^2 = p_c \frac{p_c + p}{(p_c - p)^2}, \quad p < p_c. \quad (2.30)$$

Thus the correlation exponent in ℓ space is 1, as in one dimension.

As in $d = 1$, the mean mass S of the finite clusters can be written as

$$S = 1 + \sum_{\ell=1}^{\infty} g(\ell). \quad (2.31)$$

Substituting (2.27) into (2.31) we find

$$S = p_c \frac{1+p}{p_c - p}, \quad p < p_c, \quad (2.32)$$

which is a simple generalization of the one-dimensional result (2.24). Accordingly, we find $\gamma = 1$ for the Cayley tree.

Next we consider $n_s(p)$, the probability that a chosen site on the Cayley tree belongs to a cluster of s sites, divided by s . In the one-dimensional chain, n_s was simply the product of the probability p^s that s sites are occupied and the probability $(1-p)^2$ that the (two) perimeter sites are empty. For one s cluster there exists only one realization.

In general, the probability of finding a cluster with s sites having t perimeter sites is $p^s(1-p)^t$, and there exist more than one realization for a cluster of s sites. Clusters with the same s may have different t . On a square lattice, for example, a cluster of three sites can have either eight or seven perimeter sites, depending on whether the three sites are in a line or form a right angle, respectively. Thus one has to define a quantity $g_{s,t}$, which gives the number of configurations for a cluster of s sites and t perimeter sites. For a cluster of three sites on the square lattice, $g_{3,7} = 4$ and $g_{3,8} = 2$. The general expression for n_s is therefore

$$n_s = \sum_t g_{s,t} p^s (1-p)^t. \quad (2.33)$$

On a Cayley tree, in contrast to the square lattice, there exists a unique relation between s and t . A cluster of one site is surrounded by z perimeter sites and a cluster of two sites is surrounded by $z + (z-2)$ perimeter sites. In general, a cluster of s sites has $z-2$ more perimeter sites than a cluster of $s-1$ sites. Denoting the number of perimeter sites of an s cluster by $t(s)$, we obtain

$$t(s) = z + (s-1)(z-2). \quad (2.34)$$

Thus for the Cayley tree, (2.33) reduces to

$$n_s(p) = g_s p^s (1-p)^{2+(z-2)s} \equiv g_s (1-p)^2 [p(1-p)^{z-2}]^s, \quad (2.35)$$

where g_s is simply the number of configurations for an s -site cluster. Note that (2.35) is general and holds for all values of p .

We are interested in the behavior of n_s near the critical concentration. To this end, we expand $p(1-p)^{z-2}$ around $p_c = 1/(z-1)$. To lowest order in $(p - p_c)$, we obtain

$$n_s(p) \sim n_s(p_c) f_s(p), \quad (2.36)$$

where $f_s(p) = (1 - [(p - p_c)^2 / 2p_c^2(1 - p_c)])^s$ decays exponentially for large s , $f_s(p) = \exp(-cs)$ and $c \sim (p - p_c)^2$. Accordingly, close to p_c , $f_s(p)$ is a function of *only* the *combined variable* $(p - p_c)s^\sigma$, with $\sigma = 1/2$. From the derivation it is clear that this result is valid for p approaching p_c from below or above. The exponent σ describes how fast the number of clusters of size s decreases as a function of s if we are above or below the threshold. At the threshold, this decay is described by the prefactor of $f_s(p)$ in (2.36). In principle, for the Cayley tree, it is possible to exactly evaluate g_s and hence $n_s(p_c)$ by combinatorial approaches. Instead of doing this, let us *assume* that $n_s(p_c)$ follows a power law [2.80]

$$n_s(p_c) \sim s^{-\tau}. \quad (2.37)$$

The exponent τ then follows from (2.26) and (2.36):

$$S = \frac{1}{p} \sum_s s^2 n_s(p) \sim \sum_s s^{2-\tau} e^{-cs} \sim \int_1^\infty s^{2-\tau} e^{-cs} ds. \quad (2.38a)$$

Substituting $z = cs$ we obtain

$$S \sim c^{\tau-3} \int_c^\infty z^{2-\tau} e^{-z} dz. \quad (2.38b)$$

For $\tau < 3$, the integral is nonsingular for c approaching zero and we obtain $S \sim |p - p_c|^{(\tau-3)/\sigma}$, or

$$\gamma = (3 - \tau)/\sigma. \quad (2.39)$$

Since $\gamma = 1$ and $\sigma = 1/2$, we obtain $\tau = 5/2$, consistent with the assumption $\tau < 3$.

Next we consider P_∞ . There exists a simple relation between n_s and P_∞ . Every site in the lattice is either (a) empty with probability $1 - p$, or (b) occupied *and* on the infinite cluster with probability pP_∞ , or (c) occupied but not on the infinite cluster with probability $p(1 - P_\infty) \equiv \sum_s sn_s$. This leads to the *exact* relation

$$P_\infty = 1 - \frac{1}{p} \sum_s sn_s, \quad (2.40)$$

which we will use to determine the exponent β . Below p_c , $\sum_s sn_s = p$ and $P_\infty = 0$.

If, as we did in (2.38), we express the sum in (2.40) by an integral, the integral is singular for c approaching zero and cannot be treated as a constant. In order to get rid of this artificial singularity, we write (2.40) in the form

$$P_\infty = \frac{1}{p} \sum_s s(n_s(p_c) - n_s(p)) + (p - p_c)/p. \quad (2.41)$$

The sum is proportional to $c^{\tau-2} \int_c^\infty z^{1-\tau} [1 - \exp(-z)] dz$. Since for small z

$[1 - \exp(-z)] \sim z$, the integral is no longer singular, and

$$P_\infty \sim c^{\tau-2} + \text{const} \times (p - p_c). \quad (2.42)$$

With c from (2.36) we obtain

$$\beta = (\tau - 2)/\sigma, \quad (2.43)$$

yielding $\beta = 1$ for the Cayley tree. Note that, for the Cayley tree, the two terms in (2.42) are of the same order in $(p - p_c)$. In regular lattices, the same treatment can be used to relate the exponents. Since there $(\tau - 2)/\sigma$ is less than 1, the first term is dominant.

As indicated by (2.26) and (2.40), the mean cluster mass, S , and P_∞ can be regarded as the second and first moments of the cluster distribution function $n_s(p)$. The zeroth moment $M_0 \equiv \sum_s n_s$ represents the mean number of clusters per lattice site. To leading order in $|p - p_c|$, M_0 scales as

$$M_0 \equiv \sum_s n_s \sim |p - p_c|^{2-\alpha}, \quad (2.44)$$

which defines the exponent α . The sum here can be calculated in the same way as above, and one easily obtains

$$2 - \alpha = (\tau - 1)/\sigma, \quad (2.45)$$

yielding $\alpha = -1$ for the Cayley tree.

It should be noticed that, in contrast to the critical concentration p_c , the exponents α , β , γ , σ , and τ are *independent* of z , a fact which reflects the universality property of the critical exponents.

As mentioned above, we expect that these exponents will be the same in all lattices with dimension $d \geq d_c = 6$. A special role is played by the exponent ν , which here characterizes the correlation length ξ_ℓ in chemical space. Since the Euclidean distance r has no meaning on the Cayley tree, we cannot determine the correlation length in r space. But the behavior of ξ in r space for $d \geq d_c$ can be obtained from the following arguments. Above the critical dimension, correlations between any two sites in the lattice are no longer relevant, and *any* path on a cluster will behave like a random walk (see,i.e., Sect. 3.2).

$$r^2 \sim \ell. \quad (2.46)$$

From (2.46) it follows immediately that $\tilde{\nu} = 1/d_{\min} = d_\ell/d_f = 1/2$ and hence $\xi \sim \xi_\ell^{1/2}$. Since $\xi_\ell \sim |p - p_c|^{-1}$, we have $\nu = 1/2$ in r space, for all lattices with $d \geq 6$. From the relation $d_f = d - \beta/\nu$ (2.8) and $\beta = 1$ we obtain $d_f = 4$ in $d = 6$, which then yields $d_\ell = 2$. Since $d_c = 6$, we expect the same fractal dimension for *all* $d \geq 6$. Thus the infinite percolation cluster at p_c , even in $d = \infty$, can be embedded in a four-dimensional space.

For a different approach for studying percolation on a Cayley tree, using the generating function method, see Appendix 2.A.

2.5 Scaling Theory

In the previous section, we introduced the quantity $n_s(p)$, which describes the distribution of s clusters per lattice site. It turned out that $n_s(p)$ plays a central role in the description of the geometric percolation transition. From $n_s(p)$ we obtained the mean cluster mass S , the correlation length ξ as well as the probability P_∞ that an occupied site belongs to the infinite cluster.

In general, in contrast to percolation on the Cayley tree and in $d = 1$, the cluster size distribution $n_s(p)$ is not known exactly. However, as we will show below (see also [2.1,6,67]), not all the information on $n_s(p)$ is needed in order to calculate the relevant quantities. What is important is the *scaling* form of $n_s(p)$, from which a scaling theory can be applied to determine the relations between the different critical exponents. First we discuss, as in the sections before, percolation on an infinite lattice, and later we consider effects of finite lattice size.

2.5.1 Scaling in the Infinite Lattice

We are interested in the region around the critical concentration (*critical region*) where the quantities related to the percolation transition show power-law behavior. When considering the Cayley tree we saw that, to lowest order in $(p - p_c)$, $n_s(p)$ was also described by power laws with the exponents σ and τ ,

$$n_s(p) \sim s^{-\tau} f_{\pm}(|p - p_c|^{1/\sigma} s), \quad (2.47)$$

where $\tau = 5/2$, $\sigma = 1/2$, and $f_{\pm}(z) = \exp(-z)$. The subscripts + and – refer to $p > p_c$ and $p < p_c$, respectively. In the Cayley tree, f was the same above and below p_c , but this is generally not the case. We will *assume* now that $n_s(p)$ retains the form of (2.47) on regular lattices, with the same exponents τ and σ below and above p_c . Like the other critical exponents, σ and τ are universal and depend only on the lattice dimension, not on the lattice structure. This is a consequence of the self-similarity in the neighborhood of p_c . In contrast to the exponents, the form of $f(z)$ need not be universal.

If we accept the *scaling ansatz* (2.47), we can calculate the mean cluster mass S and the probability P_∞ in the same way as in Sect. 2.4. In deriving the relations between σ , τ , β , and γ for the Cayley tree we did not use the analytic form of $n_s(p)$ explicitly, but rather the general scaling form (2.47). Consequently, the relations (2.39), (2.43), and (2.45) are not restricted to the Cayley tree, but hold for all cases where the scaling ansatz (2.47) is valid, i.e., for general d -dimensional systems.

To relate the correlation length exponent ν to σ and τ note that ξ is defined as the root mean square (rms) distance between occupied sites on the same finite cluster, averaged over all finite clusters, where each distance is given the

same weight. For clusters with s sites, the rms distance between all pairs of sites on each cluster, averaged over all clusters of size s , is simply

$$R_s^2 = \frac{2}{s(s-1)} \sum_{i=1}^s \sum_{j=1}^i \overline{(\mathbf{r}_i - \mathbf{r}_j)^2}, \quad (2.48)$$

and to find ξ we have to average over all cluster sizes.

Since every site on the lattice has probability sn_s of belonging to a cluster of s sites, and every site is connected with s sites (including the connection with itself), we have

$$\xi^2 = \sum_{s=1}^{\infty} R_s^2 s^2 n_s / \sum_{s=1}^{\infty} s^2 n_s. \quad (2.49a)$$

The factor s^2 here is due to the fact that the same weight is given to each pair of sites. Close to p_c , the large clusters dominate the sum in (2.49a). Since they are fractals, their mass s is related to R_s by [see (2.4)] $R_s \sim s^{1/d_f}$, and we obtain from (2.49a)

$$\xi^2 \sim \sum_{s=1}^{\infty} s^{2/d_f + 2 - \tau} f_{\pm}(|p - p_c|^{1/\sigma} s) / \sum_{s=1}^{\infty} s^{2 - \tau} f_{\pm}(|p - p_c|^{1/\sigma} s). \quad (2.49b)$$

To calculate the sums we transform them into integrals, as in Sect. 2.4. Since $2 - \tau$ is greater than -1 , the integrations are over nonsingular integrands, and to lowest order in $(p - p_c)$ the lower integration limit does not contribute to the integral. Following the same procedure as in (2.38) we obtain

$$\xi^2 \sim |p - p_c|^{-2/(d_f \sigma)}, \quad (2.50)$$

which yields the desired relation between ν , σ , and τ ,

$$\nu = \frac{1}{d_f \sigma} = \frac{\tau - 1}{d\sigma}. \quad (2.51)$$

Note that (2.51), together with (2.39), (2.43), and (2.45) (which hold also for general lattices, as will be shown below), represent *four* relations between the *six* exponents (α , β , γ , σ , τ , and ν), thus we have only two independent exponents.

A second quantity which characterizes the size of a finite cluster is the mean square cluster radius R^2 , defined as

$$R^2 = \sum_{s=1}^{\infty} R_s^2 s n_s / \sum_{s=1}^{\infty} s n_s. \quad (2.52a)$$

Here the same weight is given to each site of the cluster, and not to each pair of sites as in (2.49a). Following the treatment of (2.49) we obtain

$$R^2 \sim |p - p_c|^{-2\nu + \beta}. \quad (2.52b)$$

We will show in Chap. 3 that R^2 is an important quantity for describing diffusion in percolation systems. We show now that the correlation length defined in (2.49a) is the only characteristic length scale of percolation.

Using (2.51), the argument $z = |p - p_c|^{1/\sigma} s$ of the scaling function $f_{\pm}(z)$ can be written as $z = s/\xi^{d_f}$, and (2.47) becomes

$$n_s(p) \sim s^{-\tau} f_{\pm}(s/\xi^{d_f}), \quad (2.53a)$$

or equivalently, using (2.51), in terms of ξ ,

$$n_s(p) \sim \xi^{-\tau d_f} (s/\xi^{d_f})^{-\tau} f_{\pm}(s/\xi^{d_f}) = \xi^{-d-d_f} F_{\pm}(s/\xi^{d_f}), \quad (2.53b)$$

where $F_{\pm}(z) = z^{-\tau} f_{\pm}(z)$. Equations (2.53a,b) show that the correlation length ξ represents the only characteristic length scale near the percolation threshold: the cluster distribution function $n_s(p)$ depends on s via only the ratio s/ξ^{d_f} or, on replacing s by $R_s^{d_f}$, on only the ratio R_s/ξ .

It can easily be checked that the sums calculated so far are special cases of the more general expression

$$M_k = \sum_{s=1}^{\infty} s^k n_s(p) \sim \sum_{s=1}^{\infty} s^{k-\tau} f_{\pm}(s/\xi^{d_f}), \quad (2.54a)$$

from which all relations between the exponents can be obtained. The sum is transformed into the integral

$$M_k \sim \int_1^{\infty} s^{k-\tau} f_{\pm}(s/\xi^{d_f}) ds \sim \xi^{d_f(k-\tau+1)} \int_{\xi^{-d_f}}^{\infty} z^{k-\tau} f_{\pm}(z) dz. \quad (2.54b)$$

As long as the integrand is nonsingular, $k - \tau > -1$, the lower integration limit can be extended to zero, yielding

$$M_k \sim \xi^{d_f(k-\tau+1)} \sim |p - p_c|^{(\tau-1-k)/\sigma}. \quad (2.55)$$

For $k < \tau - 1$ this procedure does not work, since the lower limit dominates the integral. In this case, one can consider derivatives of M_k with respect to ξ^{-d_f} :

$$\frac{d^n M_k}{(d\xi^{-d_f})^n} \sim \xi^{d_f(k-\tau+n+1)} \int_{\xi^{-d_f}}^{\infty} z^{k-\tau+n} \frac{d^n f(z)}{dz^n} dz, \quad (2.56a)$$

where n is the smallest integer greater than $\tau - k - 1$. The integrand in (2.56a) is nonsingular and hence

$$\frac{d^n M_k}{(d\xi^{-d_f})^n} \sim \xi^{d_f(k-\tau+n+1)}. \quad (2.56b)$$

From (2.56b), we can obtain by simple integration, up to lowest-order terms,

$$M_k \sim \xi^{d_f(k-\tau+1)} \sim |p - p_c|^{(\tau-1-k)/\sigma}, \quad (2.57)$$

which shows that (2.55) is also valid for $k > \tau - 1$. From (2.57) we obtain $M_0 \sim |p - p_c|^{(\tau-1)/\sigma} \sim |p - p_c|^{2-\alpha}$ and $M_1 \sim |p - p_c|^{(\tau-2)/\sigma} \sim |p - p_c|^\beta$, which yields relations (2.45) and (2.43) between the exponents. Similarly, we obtain for $k = 2$ relation (2.39), $\gamma = (3 - \tau)/\sigma$. These three relations constitute, together with (2.51), $d\nu = (\tau - 1)/\sigma$, four relations between the six exponents. From (2.51), (2.39), and (2.43) one obtains

$$d\nu = 2\beta + \gamma, \quad (2.58)$$

a relation which has been found useful by Toulouse [2.77] to obtain the upper critical dimension d_c for percolation. At d_c , $\nu = 1/2$, $\beta = 1$, and $\gamma = 1$ (see Sect. 2.2), and hence $d_c = 6$. The same argument leads to $d_c = 4$ in Ising systems, where $\beta = 1/2$ at the critical dimension.

2.5.2 Crossover Phenomena

From the scaling form (2.53a) we learned that the correlation length ξ is the only characteristic length scale in percolation. Above p_c , ξ is finite, and we expect different behavior on length scales $r < \xi$ and $r > \xi$. In the following we present a scaling theory that describes the crossover behavior in several quantities such as P_∞ , $M(r)$, $M(\ell)$, and $R(\ell)$. First we consider the probability P_∞ that an occupied site belongs to the infinite cluster. To determine P_∞ we choose subsystems of linear size r and determine the fraction of sites in this system that belong to the infinite cluster. If $r \gg \xi$, the system behaves as if $r = \infty$, and P_∞ is independent of r and described by $P_\infty \sim (p - p_c)^\beta$. If $r \ll \xi$, on the other hand, the number of sites of the infinite cluster within a circle of radius r is proportional to r^{d_f} . The total number of occupied sites within r is proportional to pr^d , and hence $P_\infty \sim r^{d_f-d}$. Since ξ is the only characteristic length, we can assume that P_∞ depends on r and ξ via only the ratio r/ξ . This leads, in close analogy to (2.53), to the scaling ansatz

$$P_\infty \sim (p - p_c)^\beta G(r/\xi) \sim \xi^{-\beta/\nu} G(r/\xi). \quad (2.59)$$

The scaling function G describes the crossover from $r/\xi \ll 1$ to $r/\xi \gg 1$. In order to obtain the expected results in the two limits, we must require that

$$G(x) \sim \begin{cases} x^{d_f-d}, & x \ll 1, \\ \text{const}, & x \gg 1. \end{cases} \quad (2.60)$$

From (2.60) we can determine how the mean mass M of the infinite cluster scales with r and ξ above p_c . Since $M \sim r^d P_\infty(r, \xi)$, the mean mass of the infinite cluster scales as

$$M \sim r^{d-\beta/\nu} H(r/\xi), \quad H(x) = x^{\beta/\nu} G(x), \quad (2.61)$$

and we recover (2.5) and (2.8). Equations (2.60) and (2.61) generalize (2.4) for $p \geq p_c$.

Next we consider how M scales with the chemical length above p_c . Substituting (2.10), $r \sim \ell^{\bar{\nu}}$, into (2.61) gives [2.50]

$$M \sim \ell^{\bar{\nu}(d-\beta/\nu)} g(\ell/\xi_\ell), \quad (2.62)$$

where ξ_ℓ is the correlation length in ℓ space. From (2.10), (2.61), and (2.62) we obtain the scaling function $g(x)$,

$$g(x) \sim \begin{cases} \text{const}, & x \ll 1, \\ x^{d-d_f \bar{\nu}}, & x \gg 1. \end{cases} \quad (2.63)$$

Equations (2.62) and (2.63) generalize (2.9).

Finally we study how the average Euclidean distance r between sites separated by a fixed chemical distance ℓ scales above p_c . By scaling arguments similar to those given above we expect that r scales as

$$r \sim \ell^{\bar{\nu}} f(\ell/\xi_\ell), \quad (2.64)$$

where

$$f(x) \sim \begin{cases} \text{const}, & x \ll 1, \\ x^{1-\bar{\nu}}, & x \gg 1. \end{cases} \quad (2.65)$$

Equations (2.64) and (2.65) generalize (2.10) for $p > p_c$. Accordingly, at large Euclidean distances ($r > \xi$) the chemical distance and the Euclidean distance have the same metric, and [2.14,83]

$$r \sim \xi_\ell^{\bar{\nu}-1} \ell \sim \xi^{(\bar{\nu}-1)/\bar{\nu}} \ell \sim (p - p_c)^{\nu(1/\bar{\nu}-1)} \ell. \quad (2.66)$$

Equations (2.64–66) will be shown to be useful for describing spreading phenomena in Sect. 2.6.

Scaling assumptions can also be used to treat various quantities at criticality. Examples are the probability densities $\phi(M | r)$, $\phi(M | \ell)$, and $\phi(r | \ell)$, which at p_c scale as $\phi(M | r) \sim (1/M)f(M/r^{d_f})$, etc., see (2.12). Similar quantities have also been studied for the percolation backbone [2.84] and scaling theory has been successfully applied to study the blob-size distribution [2.85]. More examples (related to transport properties) are given in Chap. 3.

So far, we have considered percolation on infinitely extended lattices. In the next subsection we will use the above results to study the effect of *finite* lattices.

2.5.3 Finite-Size Effects

Consider a finite system, e.g., a triangular lattice of $L \times L$ sites, where each bond has unit length $a = 1$. We expect that the relevant quantities depend on the magnitude of L . Since the characteristic length of the system is the correlation length ξ (which is defined for the infinite system), we expect different behavior for $L/\xi \gg 1$ and for $L/\xi \ll 1$.

First consider again P_∞ . For $L \gg \xi$, the system behaves as if $L = \infty$, i.e., P_∞ is independent of L and described by $P_\infty \sim (p - p_c)^\beta$. For $\xi \gg L \gg 1$, the number of sites of the infinite cluster in the $L \times L$ “window” is proportional to L^{d_f} . We obtain P_∞ by dividing this result by the total number of occupied sites in the window, which is pL^d , hence $P_\infty \sim L^{d_f - d}$. Since ξ is the only characteristic length, P_∞ depends on L via only the ratio L/ξ , which in analogy to (2.59) leads to the scaling ansatz

$$P_\infty \sim (p - p_c)^A G(L/\xi) \sim \xi^{-A/\nu} G(L/\xi). \quad (2.67)$$

The scaling function $G(x)$ describes the crossover from $L/\xi \ll 1$ to $L/\xi \gg 1$. In order to obtain the expected results in both regimes, we must have $A = \beta$ and

$$G(x) \sim \begin{cases} x^{d_f - d}, & x \ll 1, \\ \text{const}, & x \gg 1. \end{cases} \quad (2.68)$$

To see the consequences of these relations, assume that we are going to perform computer simulations of P_∞ on the triangular lattice, where the critical concentration is exactly 1/2 (for site percolation on the infinite lattice). We choose a large lattice, say $L = 1000$, and occupy randomly all sites with probability p . Next we analyze the clusters and determine the size of the infinite cluster (if it exists). We repeat the calculations say for 5000 lattice configurations, and average P_∞ over all configurations. For p well above the percolation threshold, where ξ is considerably smaller than $L = 1000$, we do not notice the finite size of the lattice. Accordingly, if we approach p_c more closer, P_∞ will decrease as $(p - p_c)^\beta$, as long as $L \gg \xi$. If we approach p_c more and more closely we will reach a crossover concentration p^* , where $L \sim \xi$. Between p^* and p_c , $L < \xi$ and P_∞ remains roughly constant at a finite value.

This behavior can be understood as follows. In the *finite* system of 10^6 sites a small change in concentration is equivalent to adding or subtracting, on average, only a few occupied sites, which leaves the system practically unchanged. In our lattice we cannot see a difference in P_∞ for $p = p_c + 10^{-6}$ and $p = p_c + 10^{-12}$. The small change in concentration becomes more effective if we take larger systems, and for the infinite system drastic changes also occur very close to p_c . In the above example, P_∞ decreases by a factor $10^{6\beta}$ which is of the order of 10. It is obvious that the finite-size effects described here for P_∞ occur also in the cluster site distribution $n_s(p)$ and the other related quantities.

It is convenient to write the scaling relation (2.67) also in a slightly different way. Multiplying and dividing (2.67) by $L^{-\beta/\nu}$ we obtain

$$P_\infty \sim L^{-\beta/\nu} H(L/\xi), \quad (2.69)$$

where $H(x) = G(x)x^{\beta/\nu}$, as in (2.61).

From the finite-size scaling we can learn that in principle there are two ways to determine a critical exponent x of some quantity X , $X \sim (p - p_c)^{-x}$, by computer simulations. Instead of determining X , e.g., P_∞ or S , directly as a

function of $(p - p_c)$, one can calculate X right at p_c for various system sizes. This way one obtains $X \sim L^{x/\nu}$, and if ν is known, one finds x .

Using extensive computer simulations, Ziff [2.35] studied how the critical concentration depends on the linear size L of the system. He finds for large L in $d = 2$ that

$$p_c(L) = p_c(\infty) + \text{const} \times L^{-1-1/\nu}. \quad (2.70)$$

Hence, for obtaining accurate estimates for $p_c \equiv p_c(\infty)$ one has to plot $p_c(L)$ versus $x = L^{-1-1/\nu}$ and to extrapolate to $x = 0$.

A further interesting result is that the probability $R_L(p_c)$ for finding a spanning cluster at p_c (in the site percolation) approaches $1/2$ for L approaching infinity. Since this result is the same as for bond percolation, it suggests that $R_L(p_c)$ is a universal quantity that depends on only the dimension d of the system, not on the type of the lattice considered. Further numerical support for this hypothesis was obtained recently by Stauffer *et al.* [2.86] for 3d percolation, where $R_L(p_c) \cong 0.42$.

2.6 Related Percolation Problems

In this section we consider modifications of the percolation problem which are useful for describing several physical, chemical, and biological processes, such as the spreading of epidemics or forest fires, gelation processes, and the invasion of water into oil in porous media, which is relevant for the process of recovering oil from porous rocks. In some cases the modification changes the universality class of percolation. We begin with an example in which the universality class does not change.

2.6.1 Epidemics and Forest Fires

The simplest model for an epidemic disease or a forest fire is the following [2.12,15] (see also Chap. 4). On a large square lattice, each site represents an individual which can be infected with probability p and which is immune with probability $(1 - p)$. At an initial time $t = 0$ the individual at the center of the lattice (seed) is infected. We assume now that in one unit of time this infected site infects all nonimmune nearest-neighbor sites. In the second unit of time, these infected sites will infect all their nonimmune nearest-neighbor sites, and so on. In this way, after t time steps all nonimmune sites in the ℓ th chemical shell around the seed are infected, i.e., the maximum length ℓ of the shortest path between the infected sites and the seed is $\ell \equiv t$. The process of randomly infecting individuals is exactly the same as that of randomly occupying sites in the site percolation discussed in Sect. 2.1, but instead of many clusters being generated on a lattice only single clusters are formed from each seed (see also

the Leath method, Sect. 2.7). Below p_c , only finite clusters can be generated and the disease stops spreading after a finite number of time steps. Above p_c , there exists a finite probability that the disease continues for ever.

Accordingly, at p_c the mean number of infected individuals at time t is determined by the graph dimension d_ℓ (see Sect. 2.3),

$$M(t) \sim t^{d_\ell}, \quad t \gg 1. \quad (2.71)$$

The spreading radius of the disease is related to $M(t)$ by d_f , $R(t) \sim M(t)^{1/d_f}$.

Above p_c , for $R \gg \xi$, $d_\ell = d_f = 2$ and the spreading of the epidemic is characterized by the velocity v of the epidemic front; by definition $v \equiv dR/dt \sim t^{d_\ell/d_f - 1}$. It is clear from (2.71) and $d_\ell < d_f$ that $v \rightarrow 0$ at p_c and $v > 0$ above p_c . To derive the dependence of v on $p - p_c$ note that $R(t)$ can be written as [see (2.64)]

$$R(t) \sim t^{d_\ell/d_f} f(t/t_\xi), \quad (2.72)$$

where t_ξ is the characteristic time scale in the process. Since the correlation length ξ is the only characteristic length scale here, we can associate t_ξ with the time needed to generate a cluster of size ξ . For $r < \xi$ the cluster is self-similar, and we obtain from (2.71) $t_\xi \sim \xi^{d_f/d_\ell}$. For $t \ll t_\xi$, $R(t)$ is proportional to t^{d_ℓ/d_f} and f is constant. For $t \gg t_\xi$, the system is homogeneous and $R(t)$ is linear in t . In order to satisfy this relation, we require that the right-hand side of (2.72) is also linear in t , which yields $f(t/t_\xi) \sim (t/t_\xi)^{1-d_\ell/d_f}$ and $R(t) \sim t_\xi^{d_\ell/d_f - 1} t \sim \xi^{1-d_f/d_\ell} t$. Hence the spreading velocity of the disease is also described by a critical exponent [2.83],

$$v \sim \xi^{1-d_f/d_\ell} \sim (p - p_c)^{(1/\tilde{\nu} - 1)\nu}. \quad (2.73)$$

Since in $d = 2$ the exponent $(1/\tilde{\nu} - 1)\nu$ is much smaller than 1, a relatively large velocity occurs just above p_c , and the spreading transition at p_c is abrupt rather than smooth.

In the above model, an infected site infects *all* its nonimmune nearest-neighbor sites. In an improved version of the model [2.14,87] (see also [2.15]), an infected site can infect its nearest-neighbors only with probability q and within a certain time interval τ which we take as unit time (see Fig. 2.13). It is easy to see that in the absence of immune sites, i.e., $p = 1$, this model corresponds to bond percolation, since the process of randomly infecting individuals is equivalent to the process of randomly occupying bonds (and the sites connected by them). For $p < 1$, the model is equivalent to site–bond percolation (see Sect. 2.1) where only those bonds connecting occupied sites can be occupied.

We would like to note that this simple model already combines essential features of real epidemics and emphasizes the importance of the protection, here characterized by the parameter q . For small q below the percolation threshold, the epidemic cannot spread and dies out. In AIDS, for example, the virus is

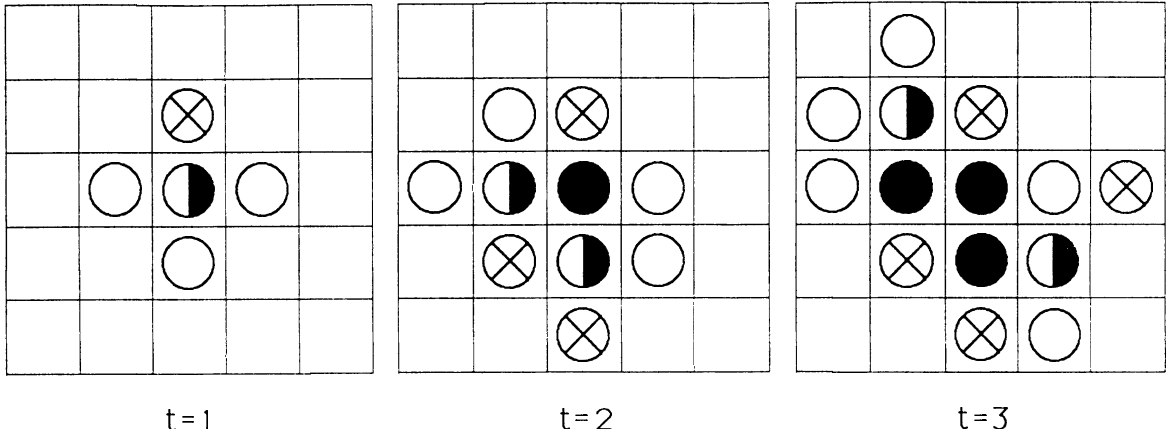


Fig. 2.13. The first three steps of the spreading of an “epidemic”. The open circles represent “nonimmune” individuals, the crosses represent the “immune” individuals, the half-full circles are the “infected” sites which are still “contagious”, and the full circles denote those infected individuals which are no longer contagious

mainly transferred by blood contacts, and q can be decreased drastically by choosing the proper type of protection.

There are several other models for spreading phenomena in dilute media. In a variant of the Eden model [2.88], one starts with a lattice consisting of immune and infectable individuals as before, with a seed in the center of the lattice. The infection spreads from the seed by randomly choosing one of the nonimmune nearest-neighbor sites of the spreading cluster (“growth sites”) and converting it into a cluster site. This process is repeated up to the desired number of time steps. Here again, the structure of the spreading clusters is described by percolation, but the dynamical features depend on how time is associated with this process. There are two choices: (a) if a new site is added to the cluster, the time is increased by one unit; (b) if a new site is added to the cluster, the time is increased by $\Delta t = 1/P$, where P is the number of growth sites in the previous step, before the new site was chosen. In the second way, in one unit of time all available growth sites can, on average, be occupied, a process that is similar to the epidemic model above. Note, however, that here an infected site is contagious for ever, i.e., it can still infect an infectable nearest-neighbor individual even after many time steps. If this condition is relaxed, and an infected site is contagious only for a finite time range τ , the dynamical process is changed completely. There exists a *critical* lifetime $\tau_c(p)$ which depends explicitly on the concentration p of the infectable species. For $p \geq p_c$ and $\tau > \tau_c$, percolation clusters are generated, while for $p \geq p_c$ and $\tau < \tau_c$ the generated clusters belong to the universality class of self-avoiding walks, with $d_f = 4/3$ in $d = 2$ [2.89].

For related models for forest fires, which exhibit features of self-organized criticality (Chap. 2 in [2.22]) we refer the reader to [2.90,91].

Next we discuss further models for spreading phenomena in dilute media, which to some extent can be also related to percolation theory.

2.6.2 Kinetic Gelation

The gelation process describes the transition from a solution containing only small molecules to a gel state where a large molecule of the size of the system is formed [2.12,13,17]. This transition is called a sol-gel transition and separates two phases with very different physical properties. The shear viscosity diverges when the transition is approached from the sol phase. Gels occur in biological systems (e.g., eye humor), and play an important role in chromatography, in the fabrication of glues and cosmetics, and in food technology (yoghurts, gelatine, etc.).

During the gelation process, chemical bonds between neighboring molecules become activated and connect the molecules to form larger and larger clusters. There exist different mechanisms for activating the bonds. Here we concentrate on the so-called addition polymerization, where unsaturated electrons hop between the molecules and create bonds.

For this process, the following kinetic gelation model was suggested by Manneville and de Seze [2.92], which is related to the percolation problem. In this model, one considers, for example, a square lattice where sites are occupied randomly by monomers with probability p and by solvent molecules with probability $(1 - p)$. Each monomer has a certain “functionality” f which states how many of its bonds can be activated ($f=1,2,3,4$ on the square lattice). Next a small concentration of initiators, modeling unsaturated electrons, are placed randomly on the monomers. The role of these initiators is to activate the available bonds between monomers by a random walk process (see Sect. 3.2). A randomly chosen initiator attempts to jump randomly to a nearest-neighbor site. If this site is a monomer with functionality $f \geq 1$, the jump is successful, the functionality is reduced by 1, and the bond between both monomers is activated. If the attempted site is a monomer with $f = 0$ or a solvent molecule, the jump is rejected. In both cases the time is increased by $1/N_i(t)$, where $N_i(t)$ is the number of initiators present at this time t . If two initiators meet at the same monomer, they annihilate. Accordingly, the concentration of initiators decreases monotonically with time t , but in general it will not reach zero since initiators surrounded by monomers with functionality zero are trapped.

The concentration $p(t)$ of occupied bonds increases with t . There exists a critical concentration p_c at which a spanning cluster exists for the first time and the gel is formed. As in normal percolation, the critical behavior of this geometric transition is described by the exponents ν and β .

Using Monte Carlo simulations it has been shown [2.93] that ν and β are the same as for normal percolation. This implies that d_f is also unchanged. In contrast, the fractal dimension of the backbone of the gel at p_c is $d_B \cong 2.22$ in $d = 3$ and differs considerably from the value 1.74 found in ordinary percolation [2.94,95].

2.6.3 Branched Polymers

The polymerization process, i.e., the generation of long polymers from monomers, has become an important topic in both applied and basic research [2.11,12,42,96–99]. It is commonly accepted that long polymer chains can be modelled by kinetic growth walks (KGW), where at each step a random walker moves only to those neighboring sites that have not been visited before [2.12]. Very recently, in order to generate branched polymer structures, Lucena *et al.* [2.102] generalized this KGW model to include branching (branched polymer growth model – (BPGM)).

The BPGM generates a branched polymer from a seed in a self-avoiding manner similar to the KGW, but allows for the possibility of branching with bifurcation probability b . To be specific, consider a square lattice where at $t = 0$ the center of the lattice is occupied by a polymer “seed”. There are four empty nearest-neighbor sites of the seed, where the polymer is allowed to grow. At step $t = 1$, two of these four growth sites are chosen randomly: one of them is occupied by the polymer with probability 1, the other one is occupied with probability b . This process is continued. At step $t+1$, the polymer can grow from each of the sites added at the step t to empty nearest-neighbor sites (growth sites) either in a linear fashion or by bifurcation with probability b , provided there are enough growth sites left; otherwise the polymer stops growing. It is clear that large polymers can be generated only for q below the percolation threshold q_c of the considered lattice ($q_c \approx 0.40723$ on the square lattice).

The structure generated by this procedure depends crucially on the branching parameter b and the impurity concentration q . For small b and large q , the structures are finite and belong to the universality class of KGW, while for large b and small q , compact Eden clusters (see Sect. 2.6.1) are generated. There exists a critical line $b_c(q)$ [2.38,102] that separates both phases (see Fig. 2.14). Numerical results suggest [2.28] that at the critical line the structures belong to the universality class of percolation, which is controversial with the earlier common belief that branched polymers are in the universality class of lattice animals [2.101].

Three interesting points should be mentioned. (i) In the considered square lattice, in the absence of impurities, the phase transition between both structures occurs at a *finite* value of the branching probability ($b > b_c(0) \cong 0.055$) [2.102]. For higher dimensions, numerical results suggest that $b_c(0) = 0$ [2.103]. (ii) For $b = 1$, the phase transition occurs at $q'_c < q_c$ (see Fig. 2.14), since an additional finite concentration of sites ($q_c - q'_c$) are blocked when the branching (here two branches at each step) is below the maximum possible branching (here three branches) on the considered lattice. (iii) Since the generated clusters are loopless, the dynamical exponents are not the same as those of lattice percolation (see Sect. 3.6).

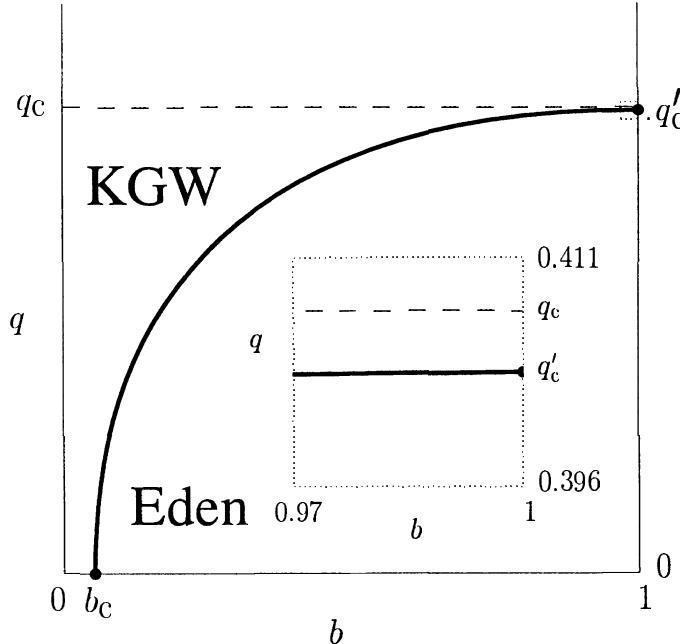


Fig. 2.14. The phase diagram for the BPGM

2.6.4 Invasion Percolation

Consider the flow of water into a porous rock filled with oil. Water and oil are two incompressible immiscible fluids and hence the oil is displaced by the water when the water invades the rock. The porous medium can be considered as a network of pores which are connected by narrow throats. The flow rate is kept constant and very low so that viscous forces can be neglected compared to capillary forces. The invasion percolation was introduced as a model to describe this dynamical process [2.104–106] (see also Sects. 4.3.3 and 7.4.2).

In the model, we again consider a regular lattice of size $L \times L$, which here represents the oil (the “defender”). Water (the “invader”) is initially placed along one edge of the lattice. To describe the different resistances of the throats to the invasion of the water we assign to each site of the lattice a random number between 0 and 1. The invading water follows the path of lowest resistance. At each time step that perimeter site of the invader which has the lowest random number is occupied by the water and the oil is displaced (see Fig. 2.15).

Since oil and water are incompressible and immiscible fluids, oil that is surrounded completely by water cannot be replaced and oil can be trapped in some regions of the porous medium. Thus, if by the Monte Carlo process a closed loop is generated the invader can no longer enter this region.

The fractal dimension of the clusters of water was found numerically to be $d_f \cong 1.82$ [2.106,108]. Experiments on air slowly invading a $d = 2$ network of ducts with glycerol performed by Lenormand and Zarcone [2.109] yielded $d_f \cong 1.8$, in good agreement with the numerical results. This value of d_f suggests that the invasion percolation model is in a universality class different from regular

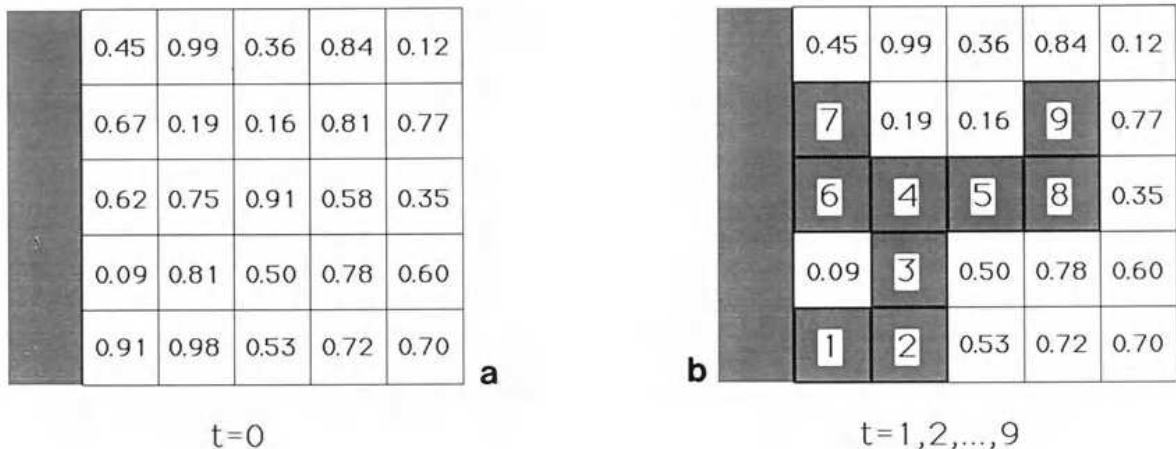


Fig. 2.15. Invasion percolation on a 5×5 square lattice (a) at the initial time and (b) after 15 time steps

percolation. Support for this conclusion comes from recent numerical results for the chemical dimension yielding $d_\ell = 1.40 \pm 0.07$ (or $\tilde{\nu} = 1/d_{\min} \cong 0.77$) [2.110]. This value for d_ℓ is significantly smaller than that of percolation (see Table 2.3).

On the other hand, if the defender is compressible, closed regimes can continue to grow and the fractal dimension of the invading fluid is larger [2.106], $d_f \cong 1.89$ ($d = 2$) and $d_f \cong 2.5$ ($d = 3$), in close agreement with percolation. For a further discussion and the relation to aggregation and viscous fingering, we refer the reader to Chaps. 4 and 7. For a recent application of invasion percolation to the invasion of nonwetting fluids through porous media see [2.107].

2.6.5 Directed Percolation

Directed percolation can be viewed as a model for a forest fire under the influence of a strong wind in one direction. Consider bond percolation on a square lattice at concentration p , and assign an arrow to each bond such that vertical bonds point in the positive x direction and horizontal bonds point in the positive y direction (see Fig. 2.16). To illustrate directed percolation let us now assume that each bond is a conductor where electric current is transmitted along *only* the directions of the arrows. There exists a critical concentration p_c that separates an insulating phase from a conducting phase. The critical concentration is larger than for ordinary percolation (see Fig. 2.16), $p_c \cong 0.479$ for the triangular lattice [2.111] and $p_c \cong 0.644701$ for the square lattice [2.112].

The structure of the clusters is now strongly anisotropic and two characteristic correlation lengths ξ_{\perp} and ξ_{\parallel} exist, perpendicular and parallel to the main direction, here the $x-y$ direction. This anisotropy is due to the fact that the clusters at p_c are self-affine (see Sect. 7.2.1) rather than self-similar objects. The critical behavior of both correlation lengths is described by

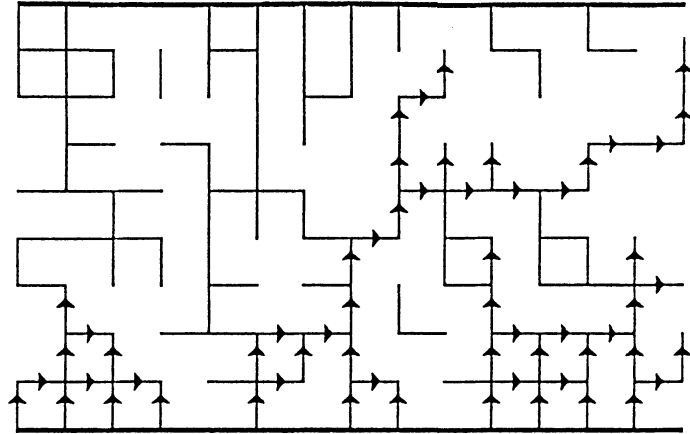


Fig. 2.16. Directed percolation on a square lattice below the percolation threshold. Although a path exists between the top and bottom lines, a current *cannot* go through. Hence the percolation threshold in directed percolation is larger than p_c in ordinary percolation

$$\xi_{\perp} \sim |p_c - p|^{-\nu_{\perp}}$$

and

$$\xi_{\parallel} \sim |p_c - p|^{-\nu_{\parallel}}, \quad (2.74)$$

with $\nu_{\perp} \neq \nu_{\parallel}$, and both are different from the exponent ν . Using scaling theory the following relation can be derived:

$$\gamma + 2\beta = (d - 1)\nu_{\perp} + \nu_{\parallel}, \quad (2.75)$$

which is a generalization of (2.58). Substituting the mean field exponents $\gamma = \beta = \nu_{\parallel} = 2\nu_{\perp} = 1$ in (2.75) yields the upper critical dimension $d_c = 5$ for directed percolation [2.113]. The best estimates for the critical exponents have been achieved using 35 terms in the series expansion method [2.112] (see Sect. 2.8.2), yielding for $d = 2$, $\nu_{\parallel} = 1.7334 \pm 0.001$, $\nu_{\perp} = 1.0972 \pm 0.0006$, and $\gamma = 2.2772 \pm 0.0003$, suggesting the rational values $\nu_{\parallel} = 26/15$, $\nu_{\perp} = 79/72$, and $\gamma = 41/18$. Also β and the other static exponents differ from ordinary percolation.

Recently, progress has been made in relating directed percolation to self-organized criticality [2.114], and in calculating the spectrum of its transfer matrix [2.115] and its fractal dimension [2.116]. It has also been shown that in directed percolation hyperscaling is violated [2.118]. A detailed review on directed percolation in $d = 2$ has been given in [2.111]. An application of directed percolation to explain interface roughening in porous media [2.117] is presented in detail in Sect. 1.15. For directed percolation in $d = 3$ see [2.119].

2.7 Numerical Approaches

In this section we present several numerical approaches to generating percolation clusters and their substructures such as the backbone and the external perimeter. Percolation clusters can be generated either by the Leath method [2.120], where the percolation cluster grows in the way a simple epidemic spreads (see Sect. 2.6), or by the Hoshen-Kopelman algorithm [2.121], where all sites in the percolation system belonging to the same cluster are identified. Substructures such as the backbone and the skeleton are obtained from the percolation cluster, while the external perimeter of the cluster (in $d = 2$) is generated directly using specific self-avoiding-walk rules.

2.7.1 Hoshen-Kopelman Method

In the Hoshen-Kopelman algorithm [2.121], all sites in the percolation system are labeled in such a way that sites with the same label belong to the same cluster and different labels are assigned to different clusters. If the same label occurs at opposite sides of the system, an infinite cluster exists. In this way the critical concentration can be determined. By counting the number of clusters with s sites, we obtain the cluster distribution function.

The algorithm is quite tricky and we use a simple example to demonstrate it. Consider the 5×5 percolation system in Fig. 2.17a which we want to analyse. Beginning at the upper left corner and ending at the lower right corner, we assign cluster labels to the occupied sites. The first occupied site gets the label 1, the neighboring site gets the same label because it belongs to the same cluster. The third site is empty and the fourth one is labeled 2. The fifth site is empty.

In the second line the first site is connected to its neighbor at the top and is therefore labeled 1. The second site is empty and the third one is labeled 3.

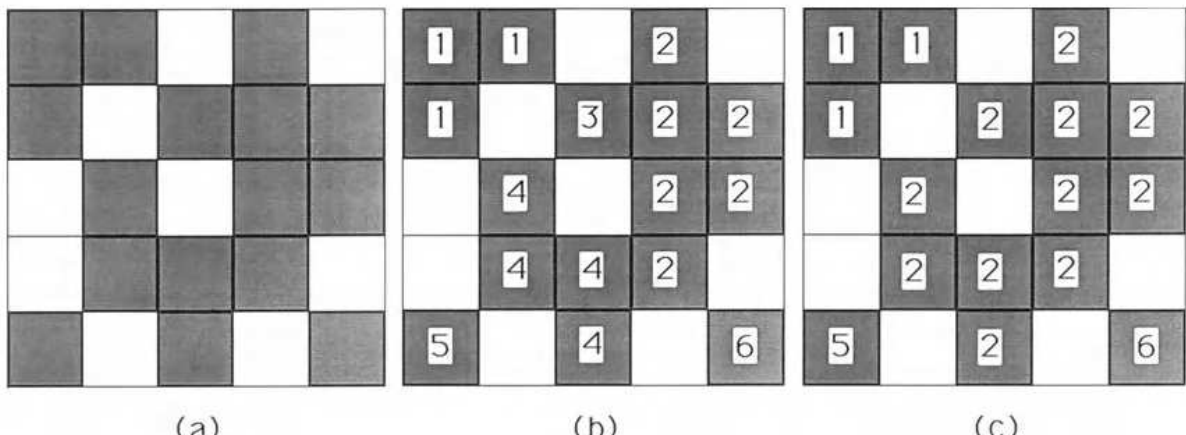


Fig. 2.17a-c. Demonstration of the Hoshen-Kopelman algorithm

The fourth site is now the neighbor of two sites, one labeled 2 and the other labeled 3. All three sites belong to the same cluster, which was first labeled 2. Accordingly, we assign the label 2 also to the new site, but we have to keep track that clusters 2 and 3 are connected. This is achieved by defining a new array $N_L(k)$: $N_L(3) = 2$ tells us that the correct label of cluster 3 is 2. If we continue the labeling we end up with Fig. 2.17b, with $N_L(3) = 2$ and $N_L(4) = 2$. Sites labeled 1, 2, 5, and 6 are not connected with sites with lower labels, and we define $N_L(1) = 1$, $N_L(2) = 2$, $N_L(5) = 5$ and, $N_L(6) = 6$.

In the second step (Fig. 2.17c) we change the improper labels [where $N_L(k) < k$] into the proper ones, beginning with the lowest improper label (here $k = 3$) and ending with the largest improper label (here $k = 4$).

The Hoshen-Kopelman algorithm is useful when investigating the distribution of cluster sizes as well as the largest cluster in any disordered system, not necessarily a percolation system. The method can also be used to determine p_c and to generate the infinite percolation cluster in percolation, but for these purposes nowadays more efficient algorithms are available, which will be described next.

2.7.2 Leath Method

In the Leath method [2.120] (see also [2.56,122]), single percolation clusters are generated in the same way as with the epidemic spreading (see Sect. 2.6). In the first step the origin of an empty lattice is occupied, and its nearest-neighbor sites are either occupied with probability p or blocked with probability $1 - p$. In the second step the empty nearest-neighbors of those sites occupied in the step before are occupied with probability p and blocked with probability $1 - p$. In each step, a new chemical shell is added to the cluster.

The process continues until no sites are available for growth or the desired number of shells has been generated. Thus, percolation clusters are generated with a distribution of cluster sizes, $s \cdot sn_s(p)$. The factor s comes from the fact that each site of the cluster has the same chance of being the origin of the cluster, and thus exactly the same cluster can be generated in s ways, enlarging the distribution $sn_s(p)$ by a factor of s . Figure 2.18 shows a cluster grown up to four shells.

The Leath method is particularly useful for studying structural and physical properties of single percolation clusters. If a large cluster is generated, the substructures like the backbone [2.70] or the skeleton [2.68] can be obtained by efficient algorithms.

2.7.3 Ziff Method

A direct method for generating the external perimeter of a percolation cluster in $d = 2$ (the hull) was suggested by Ziff *et al.* [2.123]. The method is particularly important because it also represents the most efficient algorithm

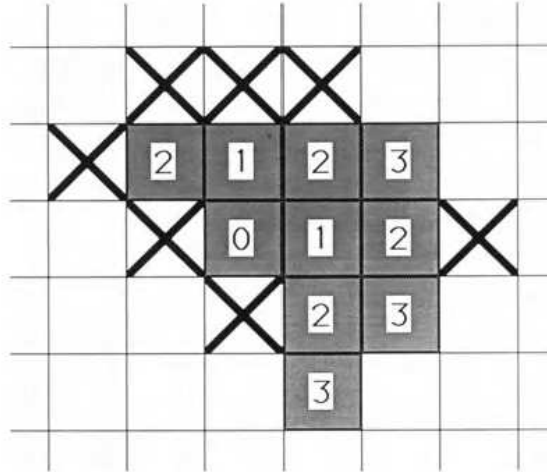


Fig. 2.18. The first four steps of the Leath cluster growth method

for determining p_c . One starts, for example, with a square lattice, where each square represents a site. First, two horizontal neighboring sites are chosen. The right one is occupied and the left is blocked (see Fig. 2.19a).

The bond between the two sites is directed along the positive y direction. This arrow represents the first step of the self-avoiding walk (SAW) by which the hull is generated. In the second step the two neighboring upper sites are considered. We begin with the right one, which is occupied with probability p and blocked with probability $1 - p$. If this site is blocked, the walk steps to the right. If the site is occupied, the left site is tested. If this is blocked the walker steps upwards; if it is occupied the walker steps to the left (see Fig. 2.19b). A new arrow is drawn accordingly and the process continues in the same way.

The method is particularly useful in $d = 2$ where only a relatively small part of the cluster is generated. It is used for determining p_c . Below p_c , finite

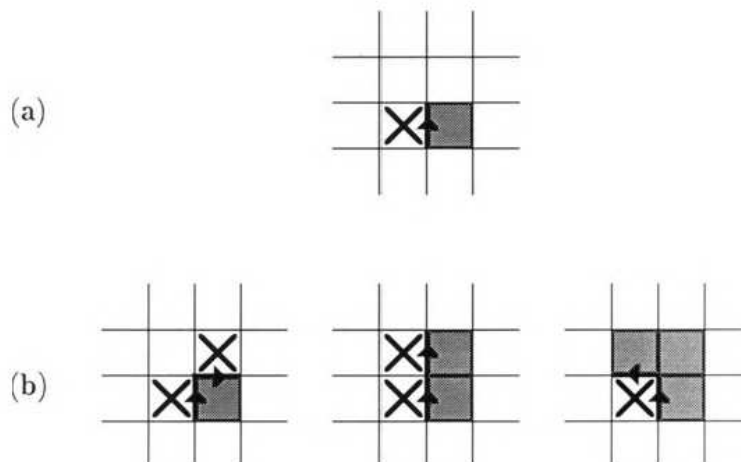


Fig. 2.19. (a) The initial step for generating the perimeter of a percolation cluster on a square lattice. (b) The three generators describing the next step. The full squares represent occupied sites and \times represents blocked sites

clusters of occupied sites dominate and closed perimeter loops in the clockwise direction will mostly be generated. Above p_c , finite clusters of empty sites dominate and closed loops of counterclockwise direction are mostly generated. At $p = p_c$ the numbers of clockwise and counterclockwise loops are equal. In this way, very accurate values of p_c can be obtained, as well as several exponents characterizing the cluster perimeter at criticality. It was shown [2.124] that these exponents are related to the correlation length exponent ν . The fractal dimension of the external perimeter is related to ν by $d_h = 1 + 1/\nu$ [2.72,73], and the distribution of clusters with perimeter length u scales as $n(u) \sim u^{-\tau}$ with $\tau = 1 + 2\nu/(1 + \nu)$. The mean perimeter length of a finite cluster diverges on approaching p_c according to $\langle u \rangle \sim (p - p_c)^{-\gamma}$ with $\gamma = 2$ [2.125].

2.8 Theoretical Approaches

Here we discuss some deterministic fractal structures which are useful for *qualitative* understanding of the fractal nature of percolation clusters, and describe the main theoretical approaches (series expansions and renormalization techniques), by which a *quantitative* description of the percolation transition can be achieved.

2.8.1 Deterministic Fractal Models

a) Sierpinski gasket. The Sierpinski gasket (see Figs. 1.1,2 in Chap. 1) was suggested [2.126] as a model for the backbone of the infinite percolation cluster at p_c . Both structures contain loops of all length scales and are *finitely ramified* [2.45], i.e., parts of them of *any* size can be isolated from the rest by cutting only a *finite* number of bonds.

The fractal dimension of the gasket is $d_f = \ln 3 / \ln 2 = 1.585$ for $d = 2$ and $d_f = \ln(d+2) / \ln 2$ for general d . In $d = 2$ and $d = 3$, d_f is thus very close to the fractal dimension of the percolation backbone, see Table 2.3. However, there the similarity ends. Other exponents, such as the graph dimension $d_\ell (= d_f)$ and the fractal dimension of the red bonds $d_{\text{red}} (= 0)$, show that the structure of the Sierpinski gasket is very different from the structure of the percolation backbone. Moreover, while in percolation the effect of loops decreases with increasing dimension, the effect of loops increases in the gasket.

The main advantage of the Sierpinski gasket is that many physical properties can be calculated exactly, since the structure is finitely ramified. These exact solutions help to provide insight onto the anomalous behavior of physical properties on fractals, as will be shown in Chap. 3.

b) Mandelbrot-Given fractal. A more refined model for percolation clusters and its substructures has been introduced by Mandelbrot and Given [2.127]. The first four generations of the Mandelbrot-Given fractal are shown in Fig. 2.20.

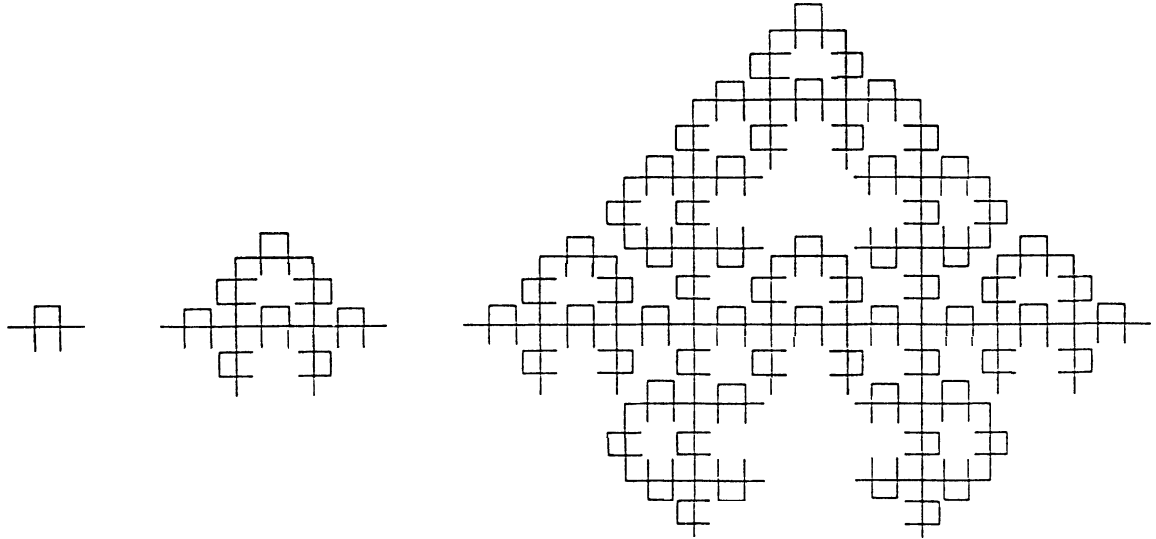


Fig. 2.20. Three generations of the Mandelbrot-Given fractal

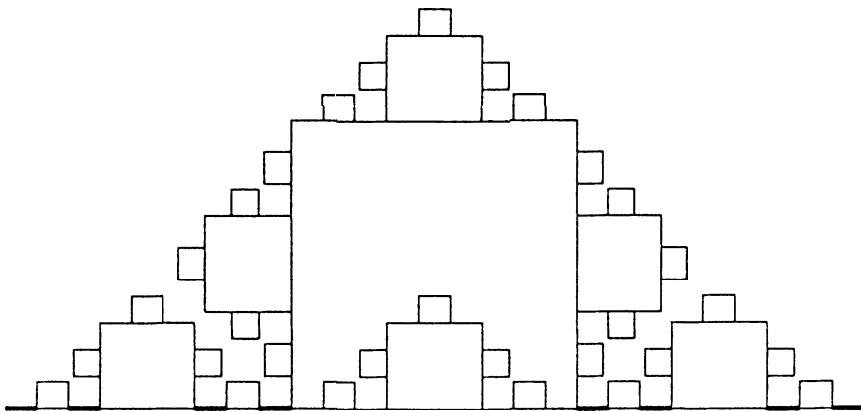


Fig. 2.21. Backbone of the Mandelbrot-Given fractal

The structure contains loops, branches, and dangling ends of all length scales. At each generation, each segment of length a is replaced by eight segments of length $a/3$. Accordingly, the fractal dimension is $d_f = \ln 8 / \ln 3 \cong 1.893$, which is very close to $d_f = 91/46 \cong 1.896$ for percolation. Note, however, that in contrast to percolation $d_{\min} = 1$ or $d_\ell = d_f$.

The backbone of this fractal can be obtained easily by eliminating the dangling ends when generating the fractal (see Fig. 2.21). It is easy to see that the fractal dimension of the backbone is $d_B = \ln 6 / \ln 3 \cong 1.63$. The red bonds are all located along the x axis of the figure and they form a Cantor set with the fractal dimension $d_{\text{red}} = \ln 2 / \ln 3 \cong 0.63$.

c) Modified Koch curve. The modified Koch curve was suggested in Chap. 1 of [2.22] as a deterministic fractal structure with a nontrivial chemical distance metric, where d_ℓ is neither 1 (as in linear fractals) nor d_f (as in the Sierpinski

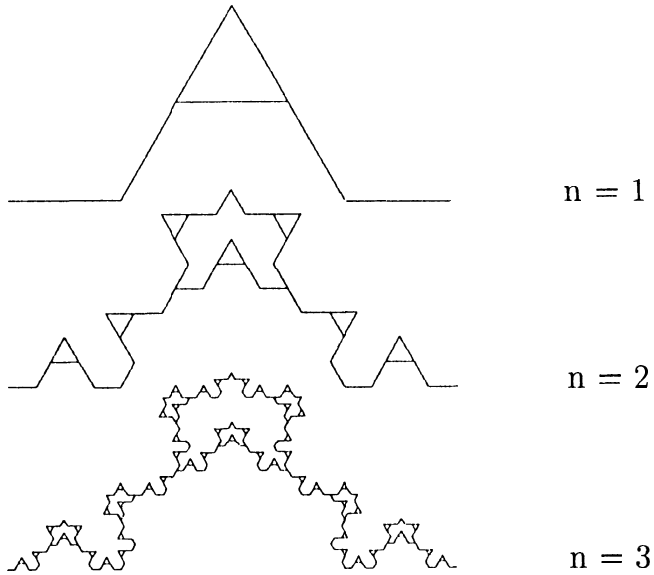


Fig. 2.22. The first iterations of a modified Koch curve, which has a nontrivial chemical distance metric

gasket or the Mandelbrot-Given fractal). The chemical distance ℓ is defined as the shortest path on the fractal between two sites of the fractal. From Fig. 2.22 we see that if we reduce ℓ by a factor of 5, the mass of the fractal within the reduced chemical distance is reduced by a factor of 7, i.e., $M(\frac{1}{5}\ell) = \frac{1}{7}M(\ell)$, yielding $d_\ell = \ln 7 / \ln 5 \cong 1.209$. It is easy to see that the fractal dimension of the structure is $d_f = \ln 7 / \ln 4 \cong 1.404$. From d_ℓ and d_f one obtains $d_{\min} = \ln 5 / \ln 4 \cong 1.161$.

d) Hierarchical model. The *hierarchical structure* (Fig. 2.23) was suggested [2.128] as a model for the percolation backbone at criticality. One starts at step $n = 0$ with a single bond of unit length. At $n = 1$ this bond is replaced

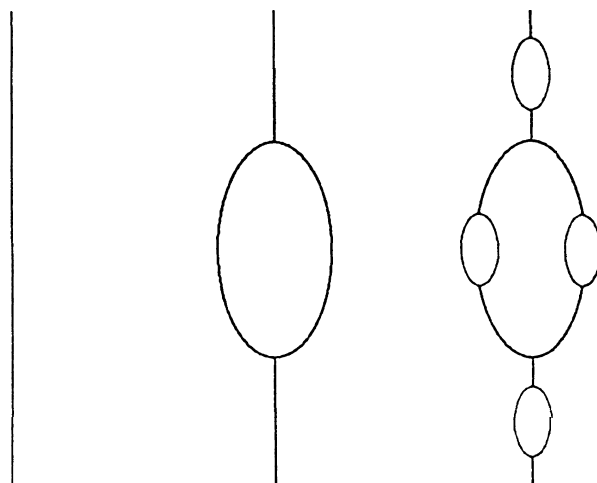


Fig. 2.23. Three generations of the hierarchical model

by four unit bonds, two in parallel and two in series. This structure, shown in Fig. 2.23, is the *unit cell*. At $n = 2$ each bond is replaced by the unit cell and this process continues indefinitely. This self-similar structure consists of blobs and singly connected bonds. The total mass of the structure is $M = 4^n$ and the number of red bonds is $n_{\text{red}} = 2^n$. In percolation $n_{\text{red}} \sim L^{1/\nu}$, see (2.18), and thus $M \sim L^{2/\nu}$ with $d_B = 1.5$ for $d = 2$ compared with $d_B = 1.62$ (Table 2.3). This model, however, gives better estimates of the dynamical exponents and, in particular, may explain the seemingly log-normal distribution in the voltage drops found in $d = 2$ percolation [2.128] (see Sect. 3.7).

Finally, we mention the *node-link-blob model* [2.51,71] for the backbone, which is essentially based on the ideas of Skal and Shklovskii [2.129] and de Gennes [2.130]. In this model, the backbone represents a superlattice network of nodes. Neighboring nodes are separated by a distance ξ , and are connected by links which include both singly connected bonds and blobs.

2.8.2 Series Expansion

The series expansion method [2.5,131] is one of the earliest techniques to determine the critical exponents for percolation. In this method, the moments M_k of the cluster distribution function [see (2.54)] are approximated by a finite power series in p (or $1 - p$),

$$M_k = \sum_{\ell=1}^{\ell_{\max}} a_\ell(k) p^\ell. \quad (2.76)$$

If we combine (2.33) and (2.54), M_k can be written as $M_k = \sum_{s,t} g_{s,t} s^k p^s (1-p)^t$, and the coefficients $a_\ell(k)$ can be expressed in terms of $g_{s,t}$ which can be calculated up to certain cluster sizes s by exactly enumerating all possible configurations. This way, for example, the first 20 terms in the expansion of the mean cluster size $S = \sum_\ell a_\ell p^\ell$ can be determined. When $p \rightarrow p_c$, S diverges and one can determine p_c and the critical exponent γ , by best fitting the series to the form $S \sim |p - p_c|^{-\gamma}$. The simplest (but not most efficient) way to do this is by expanding $(p - p_c)^{-\gamma}$ in powers of p , $(p - p_c)^{-\gamma} = \sum_{\ell=1}^{\infty} b_\ell p^\ell$. The ratio of two consecutive terms in the expansion is $b_{\ell+1}/b_\ell = (1/p_c) + [(\gamma - 1)/p_c](1/\ell)$. Thus by plotting $a_{\ell+1}/a_\ell$ as a function of $1/\ell$ one expects a straight line, the slope yields $(\gamma - 1)/p_c$ and the intercept is $1/p_c$.

This method, however, is only useful if a large number of coefficients a_ℓ are known. The reason for this is that $S(p)$ is not simply proportional to $(p - p_c)^{-\gamma}$ but also includes corrections with less divergent terms. Only for large ℓ_{\max} does the dominant contribution come from the most singular term and the approach become accurate. To improve the convergency for the (realistic) case that only few terms in the expansion are known, several quite sophisticated extrapolation techniques have been developed.

In the Padè approximation, $d \log S/dp \sim [-\gamma/(p_c - p)]$ is calculated from (2.76) by expanding $\log S(p)$, $d \log S/dp = \sum_{\ell=0}^N c_\ell p^\ell$. The polynomial is then approximated by a ratio of two polynomials, $\sum_{\ell=0}^m a_\ell p^\ell / \sum_{\ell=0}^n b_\ell p^\ell$, where $m + n = N$ is the number of the known terms in (2.76) and $b_0 = 1$. The remaining $N + 1$ coefficients a_ℓ and b_ℓ are determined from the $N + 1$ linear equations, $\sum_{\ell=0}^n b_\ell c_{j-\ell} = a_j$, where $j = 0, 1, 2, \dots, N$.

For different sets of n and m one obtains different Padè approximants for $d \log S/dp$. Since they are expected to behave as $-\gamma/(p_c - p)$, the polynomials in the denominator, $\sum_{\ell=1}^n b_\ell p^\ell$, must vanish at p_c . In general, the polynomial will have several zeros from which the most likely one is chosen as p_c ($0 < p_c < 1$). Following standard algebra, the polynomial then can be replaced by $(p_c - p) \sum_{\ell=0}^{n-1} d_\ell p^\ell$ and γ is identified as $\gamma = -\sum_{\ell=1}^m a_\ell p_c^\ell / \sum_{\ell=0}^{n-1} d_\ell p_c^\ell$. By plotting γ versus p_c for all pairs (m, n) it appears that many pairs concentrate near one point, usually around $n \cong m$, which then gives the best estimate of γ and p_c . This way, quite accurate results can be obtained. For example, one of the earliest estimations of the exponent α by Domb and Pearce [2.132] yielded $\alpha = -0.668 \pm 0.004$ for $d = 2$, which is to be compared with the exact value $\alpha = -2/3$ found several years later [2.131] (see Sect. 2.8.4). For bond percolation on the cubic lattice, the method yields $p_c = 0.2488 \pm 0.0002$. Quite accurate estimates based on 15 terms in the series expansion have been obtained also for the critical exponents in $d = 3$, $\gamma = 1.805 \pm 0.02$, $\nu = 0.872 \pm 0.023$, and $\beta = 0.405 \pm 0.025$ (see Table 2.2). For a recent pedagogical review on the method see [2.133].

2.8.3 Small-Cell Renormalization

The scaling theory discussed in Sect. 2.5 just provides relations between the critical exponents. Wilson's renormalization technique offers a method where the values of the exponents can also be studied systematically. There exist basically two variants of the method, the ϵ expansion, which is performed in reciprocal q space, and the small-cell (real-space) renormalization, which is performed in real space. In this section we will concentrate on the small cell renormalization and briefly review the ϵ expansion. The ϵ expansion is also useful for studying dynamical quantities near the percolation threshold, which will be discussed in Chap. 3.

On small scales $r < \xi$ the clusters are self-similar. Thus, if one cuts a small piece out of a cluster, and magnifies it, and compares it with the original, then one cannot decide which is the original and which is the magnification, as long as the size of the original is below ξ . At p_c , ξ diverges and we can "renormalize" the system by not looking at each site separately but by averaging over regimes of size $b \ll \xi$. If we then change the length scale accordingly, we cannot distinguish between the original and the renormalized system. This averaging procedure can be repeated again and again since $\xi = \infty$ at p_c . In this respect

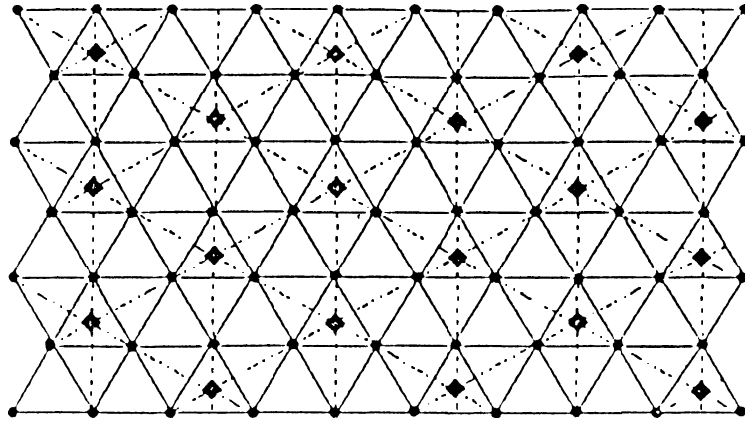


Fig. 2.24. Renormalization of a triangular lattice. The full lines represent the original lattice and the dashed lines are the renormalized one

the critical point p_c is called the mathematical “fixed point” of the renormalization transformation. If the transformation is done in the real lattice space as described here, the method is called the real-space renormalization group transformation [2.134].

Figure 2.24 shows the renormalization group transformation on a triangular lattice. Three sites form a “supersite”. The supersite is regarded as empty if the majority of the three sites (i.e. two or three sites) are empty, otherwise it is regarded as occupied. The supersites also form a triangular lattice, the lattice constant of the new lattice being $b = 3^{1/2}$. Here we assume that the lattice constant of the original lattice is 1.

In the original lattice, the correlation length behaves as

$$\xi \sim \xi_0 |p - p_c|^{-\nu}, \quad (2.77a)$$

where ξ_0 is of the order of the lattice constant. In the new superlattice, the correlation length can be written as

$$\xi' \sim \xi'_0 |p' - p_c|^{-\nu}, \quad (2.77b)$$

where $\xi'_0 = b\xi_0$ and p' is the probability that a site in the superlattice is occupied. Since the actual value of the correlation length remains unchanged by the transformation, we have $\xi' = \xi$ and hence $b|p' - p_c|^{-\nu} = |p - p_c|^{-\nu}$ or

$$\nu = \frac{\ln b}{\ln(\frac{p'-p_c}{p-p_c})}. \quad (2.78)$$

Since a site in the superlattice is occupied if either all three sites in the normal lattice are occupied (with probability p^3) or if two of them are occupied and one is empty (with probability $3p^2(1-p)$), the probability of having a supersite occupied is simply

$$p' = p^3 + 3p^2(1-p). \quad (2.79)$$

At the percolation threshold we expect $p_c = p'_c (= 1/2)$, which is satisfied by (2.79). Inserting (2.79) into (2.78) we obtain

$$\nu = \frac{\ln 3^{1/2}}{\ln 3/2} \cong 1.355,$$

in close agreement with the exact value 4/3.

At first glance it seems surprising that the result for ν is not exact. The reason lies in the fact that the renormalization transformation as described does not preserve the connectivity between the sites. Two sites which belong to the same cluster before the transformation may belong to different clusters after the transformation. Hence different transformation schemes may lead to different values of the exponents, which is a serious drawback of the renormalization group method in percolation.

Despite this, renormalization arguments have been used successfully by Coniglio [2.66,71] to determine the fractal dimension of the “red bonds”. To calculate d_{red} , consider again the original lattice with lattice constant 1 and a superlattice with lattice constant $b \gg 1$. In the superlattice, bonds between two sites are occupied if the sites are connected in the original lattice. This rule is better suited to treating percolation problems than the majority rule discussed above. At the percolation threshold, the bond concentrations in the two lattices are the same.

If we cut a small fraction q of bonds in the original lattice, a certain fraction q' of renormalized bonds becomes disconnected. The concentrations of bonds in both lattices are $p = p_c(1 - q)$ and $p' = p_c(1 - q')$, respectively, hence $q = (p_c - p)/p_c$ and $q' = (p_c - p')/p_c$.

The relation between q and q' can be obtained as follows: consider a “renormalized” bond connecting two sites on the superlattice, which by definition belong to the same cluster in the original lattice. If we cut a small fraction q of the bonds, the probability that both sites become disconnected is

$$q' = n_{\text{red}}q, \quad (q \rightarrow 0), \quad (2.80)$$

where $n_{\text{red}} \sim b^{d_{\text{red}}}$ is the number of red bonds on the backbone connecting the two sites. Equation (2.80) reflects the fact that cutting only one red bond between the two sites is sufficient to disconnect them. The probability of cutting blobs is at least of order q^2 , which can be neglected for $q \rightarrow 0$.

From (2.80) we obtain immediately $(p'_c - p) \sim b^{d_{\text{red}}} (p_c - p)$. Comparing this result with (2.78) we obtain the exact relation

$$d_{\text{red}} = 1/\nu. \quad (2.81)$$

2.8.4 Potts Model, Field Theory, and ϵ Expansion

There exist several ways to map the percolation model onto the q -state Potts model in the limit $q \rightarrow 0$ [2.135]. A common way [2.7] is to start with the dilute Ising Hamiltonian,

$$H = - \sum_{\langle i,j \rangle} J_{ij} S_i S_j, \quad (2.82)$$

where $S_i = \pm 1$ and J_{ij} are nearest-neighbor interactions which can take the value J with probability p and 0 with probability $1 - p$. The partition function is

$$Z\{J_{ij}\} = \text{Tr} \left\{ \exp \left(\beta \sum_{\langle i,j \rangle} J_{ij} S_i S_j \right) \right\}, \quad (2.83)$$

and the average free energy is

$$F = -\frac{kT}{N} \langle \ln Z\{J_{ij}\} \rangle. \quad (2.84)$$

The average $\langle \dots \rangle$ is over the quenched distribution of J_{ij} . Using the replica assumption

$$\ln Z = \lim_{n \rightarrow 0} \frac{Z^n - 1}{n}, \quad (2.85)$$

one obtains

$$\langle Z^n \rangle = \prod_{\langle ij \rangle} \exp(h_{ij}), \quad (2.86)$$

where

$$\exp(h_{ij}) = p \exp \left(\beta J \sum_{\alpha=1}^n (S_i^\alpha S_j^\alpha - 1) \right) + 1 - p. \quad (2.87)$$

The trace here is over the n replicated spins S_i^α , $\alpha = 1, \dots, n$. For $\beta J \rightarrow \infty$ (corresponding to $T \rightarrow 0$), the rhs of (2.86) takes only two values, $\exp(h_{ij}) = 1$ if $S_i^\alpha = S_j^\alpha$ for all α , and $\exp(h_{ij}) = 1 - p$ otherwise. We can therefore express h_{ij} , for $\beta J \rightarrow \infty$, by

$$h_{ij} = -\ln(1 - p) \left(\prod_{\alpha=1}^n \delta_{S_i^\alpha, S_j^\alpha} - 1 \right). \quad (2.88)$$

Equation (2.88) represents the pair interaction between sites i and j in the Hamiltonian of the q -state Potts model with $q = 2^n$ states and a coupling constant $-\ln(1 - p)$. The essential point is that by taking the limit $n \rightarrow 0$ one eliminates the property of spins, and only the geometrical connectivity is left. Thus the exponents derived for the Potts model in the limit of $n \rightarrow$

0 also represent the exponents for the pure percolation problem. From the renormalization treatment of the Potts model (which gives exact values only in $d = 2$) one finds for percolation in $d = 2$, $\nu = 4/3$, $\beta = 5/36$, $\gamma = 43/18$ and $d_f = 91/48$ [2.48,49].

The fractal dimensions of the percolation substructures like d_B and the graph dimension d_ℓ could not be derived by similar analogies.

For dimensions $d \geq 3$, the critical exponents can be estimated from the ϵ expansion. In this method, a Potts model field theory is derived using the momentum space representation of the Potts Hamiltonian, and standard momentum space renormalization methods are applied where large momentum values (corresponding to small distances) are traced out. The critical exponents are expanded in $\epsilon = 6 - d$ around the critical dimension $d = 6$. The method is tedious and only expansions up to second order in ϵ have been performed. The results are

$$\nu = \frac{1}{2} + \frac{5}{84}\epsilon + \frac{589}{37044}\epsilon^2 + O(\epsilon^3), \quad (2.89a)$$

$$\beta = 1 - \frac{1}{7}\epsilon - \frac{61}{12348}\epsilon^2 + O(\epsilon^3), \quad (2.89b)$$

and

$$d_f = d - \frac{\beta}{\nu} = 4 - \frac{10}{21}\epsilon + \frac{103}{9261}\epsilon^2 + O(\epsilon^3), \quad (2.89c)$$

which gives reasonable results for high dimensions. For example, in $d = 3$ (2.89c) yields $d_f \cong 2.67$, which is to be compared with the best numerical value 2.52.

The exponent $d_{\min} = 1/\tilde{\nu}$ was calculated by Cardy and Grassberger [2.59] up to the order of ϵ . Janssen [2.136] calculated $d_{\min} = 1/\tilde{\nu}$ up to the order of ϵ^2 , $d_{\min} = 2 - \frac{1}{6}\epsilon - [\frac{937}{588} + \frac{45}{49}(\ln 2 - \frac{9}{10}\ln 3)](\frac{\epsilon}{6})^2 + O(\epsilon^3)$, yielding $d_{\min} \cong 1.1695$, which is to be compared with the best numerical value 1.374 (see Table 2.3).

2.A Appendix: The Generating Function Method

In this appendix we present an alternative method to derive the percolation exponents on a Cayley tree. We show how the generating-function approach works in the case of classical percolation on the Cayley tree with coordination number $z = 3$, where the bonds are randomly disconnected with probability p . For each site we introduce a probability $F(s)$ that this site is connected to the branch of s bonds via a given bond. Actually $F(s)$ can be identified with sn_s defined in Sect. 2.5. Since all branches and sites on the Cayley tree are equivalent, we can write

$$F(s) = (1 - p) \sum_{s_1 + s_2 = s - 1} F(s_1)F(s_2), \quad F(0) = p. \quad (2.90)$$

To simplify this convolution sum one can use the generating function

$$f(x) = \sum_{s=0}^{\infty} F(s)x^s. \quad (2.91)$$

As shown below, simple relations exist between this generating function and the quantities of interest such as P_∞ and $\langle s \rangle$. Multiplying both sides of (2.90) by x^s and summing over s yields the quadratic equation,

$$f(x) = p + (1-p)xf^2(x), \quad (2.92)$$

with two real solutions. Taking into account that if $x \leq 1$ then $f(x) \leq 1$, we select the smaller of the two solutions,

$$f(x) = \frac{1 - \sqrt{1 - 4p(1-p)x}}{2(1-p)x}. \quad (2.93)$$

The order parameter is $P_\infty = 1 - f(1)$. At $x = 1$, the positive value of the square root is equal to $|2p - 1|$. If $p > 1/2$ then $|2p - 1| = 2p - 1$ which gives $f(1) = 1$. For p below $1/2$ we have $f(1) = p/(1-p) < 1$ and the order parameter is different from zero. Hence $p_c = 1/2$ and

$$P_\infty = 1 - f(1) = \frac{1 - 2p}{1 - p} \sim (p_c - p)^\beta, \quad (2.94)$$

with $\beta = 1$. The function $f(x)$ has a singularity at point $x_0 = 1/4p(1-p)$ of the type

$$f(x) = A + B|x - x_0|^a, \quad (2.95)$$

with $a = 1/2$. According to the Tauberian theorems [2.81], which relate singularities in $f(x)$ to singularities in $F(s)$, (2.95) suggests that the Taylor expansion of the function $f(x)$ near $x = 0$ behaves as

$$F(s) = s^{-\tau+1}\phi(s^\sigma|p - p_c|) \sim s^{-\tau+1}\exp(-s/s_c) \quad (2.96)$$

where

$$\tau = 2 + a, \quad s_c = 1/\ln(x_0). \quad (2.97)$$

Thus, in our case,

$$\tau = 5/2 \quad (2.98)$$

and

$$s_c \approx \frac{1}{x_0 - 1} = \frac{p(1-p)}{(p - p_c)^2}, \quad (2.99)$$

which gives

$$\sigma = 1/2. \quad (2.100)$$

In this simple case the function $F(s)$ can be computed according to the binomial expansion of $\sqrt{1 - y}$

$$F(s) = 2p \frac{(2s-1)!!}{(2s+2)!!} (4p(1-p))^s, \quad (2.101)$$

where the ratio of factorials has the power-law asymptotic behavior $s^{-3/2}$, and the term $(4p(1-p))^s$ gives an exponential cutoff.

We can also compute the average cluster size

$$\langle s \rangle = \sum_{s=0}^{\infty} s F(s) = df(x)/d\ln x|_{x=1}$$

and get

$$\langle s \rangle = \frac{(1-p)}{2|p - p_c|} \quad p > p_c, \quad (2.102a)$$

$$\langle s \rangle = \frac{p}{2|p - p_c|} \quad p < p_c, \quad (2.102b)$$

which means that $\gamma = 1$ on both sides.

Acknowledgements. We like to thank D. Ben-Avraham, I. Dayan, J. Dräger, H. Bolterauer, P. Maass, M. Meyer, U. A. Neumann, R. Nossal, M. Porto, S. Rabinovich, H. E. Roman, S. Schwarzer, H. E. Stanley, D. Stauffer, H. Taitelbaum, and G. H. Weiss for valuable discussions and helpful remarks.

References

- 2.1 D. Stauffer: *Introduction to Percolation Theory* (Taylor and Francis, London 1985)
- 2.2 A mathematical approach can be found in H. Kesten: *Percolation Theory for Mathematicians* (Birkhauser, Boston 1982);
G.R. Grimmet: *Percolation* (Springer, New York 1989)
- 2.3 A collection of review articles: *Percolation Structures and Processes*, ed. by G. Deutscher, R. Zallen, J. Adler (Adam Hilger, Bristol 1983)
- 2.4 S. Kirkpatrick: in *Le Houches Summer School on Ill Condensed Matter*, ed. by R. Maynard, G. Toulouse (North Holland, Amsterdam 1979)
- 2.5 C. Domb: in Ref. [2.3];
C. Domb, E. Stoll, T. Schneider: *Contemp. Phys.* **21**, 577 (1980)
- 2.6 J.W. Essam: *Rep. Prog. Phys.* **43**, 843 (1980)
- 2.7 A. Aharony: in *Directions in Condensed Matter Physics*, ed. by G. Grinstein, G. Mazenko (World Scientific, Singapore 1986)
- 2.8 A. Bunde: *Adv. Solid State Phys.* **26**, 113 (1986)
- 2.9 M. Sahimi: *Application of Percolation Theory* (Taylor and Francis, London 1993)
- 2.10 D.L. Turcotte: *Fractals and Chaos in Geology and Geophysics* (Cambridge University Press, Cambridge 1992)
- 2.11 P.G. de Gennes: *Scaling Concepts in Polymer Physics* (Cornell University Press, Ithaca 1979)
- 2.12 H.J. Herrmann: *Phys. Rep.* **136**, 153 (1986)
- 2.13 F. Family, D. Landau, eds.: *Kinetics of Aggregation and Gelation* (North Holland, Amsterdam 1984);

- For a recent review on gelation see M. Kolb, M.A.V. Axelos: in *Correlatios and Connectivity: Geometric Aspects of Physics, Chemistry and Biology*, ed. by H.E. Stanley, N. Ostrowsky, (Kluwer, Dordrecht 1990) p. 225
- 2.14 P. Grassberger: Math. Biosci., **62**, 157 (1986); J. Phys. A **18**, L215 (1985); J. Phys. A **19**, 1681 (1986)
- 2.15 G. Mackay, N. Jan: J. Phys. A **17**, L757 (1984)
- 2.16 J. Feder: *Fractals* (Plenum, New York 1988)
- 2.17 T. Vicsek: *Fractal Growth Phenomena* (World Scientific, Singapore 1989)
- 2.18 H.E. Stanley, N. Ostrowsky, eds.: *On Growth and Form: Fractal and Non-Fractal Patterns in Physics* (Nijhoff, Dordrecht 1985);
H.E. Stanley, N. Ostrowsky, eds.: *Random Fluctuations and Pattern Growth; Experiments and Models* (Kluwer, Dordrecht 1988);
H.E. Stanley, N. Ostrowsky, eds.: *Correlatios and Connectivity: Geometric Aspects of Physics, Chemistry and Biology* (Kluwer, Dordrecht 1990)
- 2.19 D. Avnir, ed.: *The Fractal Approach to Heterogeneous Chemistry* (John Wiley, New York 1989)
- 2.20 R. Zallen: *The Physics of Amorphous Solids* (John Wiley, New York 1983)
- 2.21 J.F. Gouyet: *Physics and Fractal Structures* (Springer, New York 1995)
- 2.22 A. Bunde, S. Havlin, eds.: *Fractals in Science* (Springer, Heidelberg 1994)
- 2.23 G. Dumpich, St. Friedrichowski, A. Plewnia, P. Ziemann: Phys. Rev. B **48**, 15332 (1993)
- 2.24 U. Lauer, J. Maier: Ber. Bunsenges. Phys. Chem. **96**, 111 (1992);
J. Maier: Prog. Solid St. Chem. **23**, 171 (1995)
- 2.25 M.D. Ingram: Phys. Chem. Glasses **28**, 215 (1987)
- 2.26 H. Harder, A. Bunde, W. Dieterich: J. Chem. Phys. **85**, 4123 (1986);
M.D. Ingram, M.A. Mackenzie, W. Müller, M. Torge: Solid State Ionics **40&41**, 671 (1990);
A. Bunde, M.D. Ingram, P. Maass: J. Non-Cryst. Solids **173-174**, 1222 (1994)
- 2.27 A. Bunde, W. Dieterich, H.E. Roman: Phys. Rev. Lett. **55**, 5 (1985)
- 2.28 A. Bunde, S. Havlin, M. Porto: Phys. Rev. Lett. **74** 2714 (1995)
- 2.29 R. Engelman, Z. Jaeger, eds.: *Fragmentation, Form and Flow in Fractured Media*, (Adam Hilger, Bristol 1986)
- 2.30 M. Plogzajczak, A. Tucholski: Phys. Rev. Lett. **65**, 1539 (1990)
- 2.31 P.E. Seiden, L.S. Schulman: Adv. Phys. **39**, 1 (1990)
- 2.32 H.E. Stanley, R.L. Blumberg, A. Geiger: Phys. Rev. B **28**, 1626 (1983);
R.L. Blumberg, H.E. Stanley, A. Geiger, P. Mausbach: J. Chem. Phys. **80**, 5230 (1984);
F. Sciortino, P.H. Pool, H.E. Stanley, S. Havlin: Phys. Rev. Lett. **64**, 1686 (1990)
- 2.33 J.W. Essam, D.S. Gaunt, A.J. Guttmann: J. Phys. A **11**, 1983 (1978)
- 2.34 R.M. Ziff, B. Sapoval: J. Phys. A **19**, L1169 (1987)
- 2.35 R.M. Ziff: Phys. Rev. Lett. **69**, 2670 (1992)
- 2.36 M.F. Sykes, M.K. Wilkinson: J. Phys. A **19**, 3415 (1986);
J. Adler, Y. Meir, A.B. Harris, A. Aharony: Bull. Isr. Phys. Soc. **35**, 102 (1989)
- 2.37 R.M. Ziff, G. Stell: unpublished
- P.N. Strenski, R.M. Bradley, J.M. Debierre: Phys. Rev. Lett. **66**, 133 (1991)
- 2.38 C. Domb: Proc. Phys. Soc. **89**, 859 (1966)
- 2.39 P. Grassberger: J. Phys. A **25**, 5867 (1992)
- 2.40 T. Vicsek, J. Kertesz: J. Phys. A **14**, L31 (1981);
J. Kertesz: J. Physique **42** L393 (1981)
- 2.41 W.T. Elam, A.R. Kerstein, J.J. Rehr: Phys. Rev. Lett. **52**, 1515 (1984)
- 2.42 P.J. Flory: *Principles of Polymer Chemistry* (Cornell University, New York 1971);
P.J. Flory: J. Am. Chem. Soc. **63**, 3083, 3091, 3096 (1941);
W.H. Stockmayer: J. Chem. Phys. **11**, 45 (1943)
- 2.43 S.R. Broadbent, J.M. Hammersley: Proc. Camb. Phil. Soc., **53**, 629 (1957)
- 2.44 See e.g., S.K. Ma: *Modern Theory of Critical Phenomena* (Benjamin, Reading 1976)
- 2.45 B.B. Mandelbrot: *Fractals: Form, Chance and Dimension* (Freeman, San Francisco 1977);
B.B. Mandelbrot: *The Fractal Geometry of Nature* (Freeman, San Francisco 1982)
- 2.46 H.E. Stanley: *Introduction to Phase Transition and Critical Phrenomena* (Oxford University, Oxford 1971)

- 2.47 C. Domb, J.L. Lebowitz, eds.: *Phase Transitions and Critical Phenomena* (Academic Press, New York 1972)
- 2.48 M.P.M. den Nijs: J. Phys. **12**, 1857 (1979)
- 2.49 B. Nienhuis: J. Phys. A **15**, 199 (1982)
- 2.50 S. Havlin, D. Ben-Avraham: Adv. in Phys. **36**, 693 (1987)
- 2.51 H.E. Stanley: J. Phys. A **10**, L211 (1977)
- 2.52 R.J. Harrison, G.H. Bishop, G.D. Quinn: J. Stat. Phys. **19**, 53 (1978)
- 2.53 B.H. Zimm, W.H. Stockmayer: J. Chem. Phys. **17**, 1301 (1949)
- 2.54 T.C. Lubensky, J. Isaacson: Phys. Rev. A **20**, 2130 (1979)
- 2.55 K.M. Middlemiss, S.G. Whittington, D.C. Gaunt: J. Phys. A **13**, 1835 (1980)
- 2.56 Z. Alexandrowicz: Phys. Lett. A **80**, 284 (1980)
- 2.57 R. Pike, H.E. Stanley: J. Phys. A **14**, L169 (1981)
- 2.58 S. Havlin, R. Nossal: J. Phys. A **17**, L427 (1984)
- 2.59 J.L. Cardy, P. Grassberger: J. Phys. A **18**, L267 (1985)
- 2.60 H.E. Stanley: J. Stat. Phys. **36**, 843 (1984)
- 2.61 H.J. Herrmann, H.E. Stanley: J. Phys. A **21**, L829 (1988)
- 2.62 P. Meakin, I. Majid, S. Havlin, H.E. Stanley: J. Phys. A **17**, L975 (1984)
- 2.63 S. Havlin, B. Trus, G.H. Weiss, D. Ben-Avraham: J. Phys. A **18**, L247 (1985); U.A. Neumann, S. Havlin: J. Stat. Phys. **52**, 203 (1988)
- 2.64 A. Bunde, J. Dräger: Phil. Mag. B **71**, 721 (1995); Phys. Rev. E **52**, 53 (1995)
- 2.65 H.E. Roman: Phys. Rev. E **51**, 5422 (1995)
- 2.66 A. Coniglio: J. Phys. A **15**, 3829 (1982)
- 2.67 J.F. Gouyet: Physica A **191**, 301 (1992)
- 2.68 S. Havlin, R. Nossal, B. Trus, G.H. Weiss: J. Stat. Phys. A **17**, L957 (1984)
- 2.69 H.J. Herrmann, D.C. Hong, H.E. Stanley: J. Phys. A **17**, L261 (1984)
- 2.70 (a) H.J. Herrmann, H.E. Stanley: Phys. Rev. Lett. **53**, 1121 (1984);
 (b) M.D. Rintoul, H. Nakanishi: J. Phys. A **27**, 5445 (1994)
- 2.71 A. Coniglio: Phys. Rev. Lett. **46**, 250 (1982)
- 2.72 B. Sapoval, M. Rosso, J.F. Gouyet: J. Physique Lett. **46** L149 (1985)
- 2.73 H. Saleur, B. Duplantier: Phys. Rev. Lett. **58**, 2325 (1987)
- 2.74 T. Grossman, A. Aharony: J. Phys. A **20**, L1193 (1987)
- 2.75 G. Huber, H.E. Stanley: unpublished
- 2.76 S. Havlin, J.E. Kiefer, F. Leyvraz, G.H. Weiss: J. Stat. Phys. **47**, 173 (1987)
- 2.77 G. Toulouse: Nuovo Cimento B **23**, 234 (1974)
- 2.78 S. Kirkpatrick: Phys. Rev. Lett. **36**, 69 (1976)
- 2.79 M.E. Sykes, D.S. Gaunt, H. Ruskin: J. Phys. A **9**, 1899 (1976)
- 2.80 M.E. Fisher: Physics **3**, 255 (1967)
- 2.81 G.H. Weiss: *Aspects and Applications of the Random Walk* (North Holland, Amsterdam 1994)
- 2.82 D. Stauffer: Phys. Rep. **54**, 1 (1979)
- 2.83 A.L. Ritzenberg, R.I. Cohen: Phys. Rev. B **30**, 4036 (1984);
 M. Barma: J. Phys. A **18**, L277 (1985)
- 2.84 M. Porto, A. Bunde, S. Havlin, H.E. Roman: Phys. Rev. E (1996)
- 2.85 M.F. Guyer, M.V. Ferer, B.F. Edwards, G. Huber: Phys. Rev. E **51**, 2632 (1995)
- 2.86 D. Stauffer, J. Adler, A. Aharony: J. Phys. A **27**, L475 (1994)
- 2.87 W. von Niessen, A. Blumen: Canadian Journal of Forest Research **18**, 805 (1988)
- 2.88 M. Eden: Proc. 4th Berkeley Symp. on Math. Stat. and Prob., **4**, 223 (1961);
 A. Bunde, H.J. Herrmann, A. Margolina, H.E. Stanley: Phys. Rev. Lett. **55**, 653 (1985)
- 2.89 A. Bunde, S. Miyazima: J. Phys. A **21**, L345 (1988)
- 2.90 B. Drossel, F. Schwabl: Phys. Rev. Lett. **69**, 1628 (1992);
 B. Drossel, S. Clar, F. Schwabl: Phys. Rev. Lett. **71** 3739 (1993)
- 2.91 E.V. Albano: J. Phys. A **27**, L881 (1994)
- 2.92 P. Manneville, L. de Seze: in *Numerical Methods in the Study of Critical Phenomena*, ed. by I. Della Dora, J. Demongeot, B. Lacolle (Springer, Heidelberg 1981)
- 2.93 H.J. Herrmann, D.P. Landau, D. Stauffer: Phys. Rev. Lett. **49**, 412 (1982);
 N. Jan, A. Coniglio, H.J. Herrmann, D.P. Landau, F. Leyvraz, H.E. Stanley: J. Phys. A **19**, L399 (1986)

- 2.94 A. Chhabra, D.P. Landau, H.J. Herrmann: in *Fractals in Physics*, ed. by L. Pietronero, E. Tossati (North-Holland, Amsterdam 1986)
- 2.95 D. Stauffer, A. Coniglio, A. Adam: Adv. Polymer Science **44**, 103 (1982)
- 2.96 P. Munk: *Introduction to Macromolecular Science* (Wiley, New York 1989)
- 2.97 M. Doi, S.F. Edwards: *The Theory of Polymer Dynamics* (Oxford University Press, Oxford 1986)
- 2.98 A.Yu. Grossberg, A. Khokhlov: *Statistical Physics of Macromolecules* (AIP Press, New York 1994)
- 2.99 M. Daoud, in [2.22]
- 2.100 I. Majid, N. Jan, A. Coniglio, H.E. Stanley: Phys. Rev. Lett. **52**, 1257 (1984);
K. Kremer, J.W. Lyklema: Phys. Rev. Lett. **55**, 2091 (1985);
S. Havlin, B. Trus, H.E. Stanley: Phys. Rev. Lett. **53**, 1288 (1984)
- 2.101 T.C. Lubensky, J. Isaacson: Phys. Rev. Lett. **41**, 829 (1978);
S. Havlin, Z.V. Djordjevic, I. Majid, H.E. Stanley: Phys. Rev. Lett. **53**, 178 (1984)
- 2.102 L.A. Lucena, J.M. Araujo, D.M. Tavares, L.R. da Silva, C. Tsallis: Phys. Rev. Lett. **72**, 230 (1994)
- 2.103 M. Porto, A. Shefter, A. Bunde, S. Havlin: preprint
- 2.104 R. Lenormand, S. Boris: C. R. Acad. Sci. (Paris) **291**, 279 (1980)
- 2.105 R. Chandler, J. Koplik, K. Lerman, J. Willemsen: J. Fluid Mech. **119**, 249 (1982)
- 2.106 D. Wilkinson, J. Willemsen: J. Phys. A **16**, 3365 (1983)
- 2.107 P. Meakin, G. Wagner, J. Feder, T. Jøssang: Physica A **200**, 241 (1993)
- 2.108 L. Furuberg, J. Feder, A. Aharony, I. Jøssang: Phys. Rev. Lett. **61**, 2117 (1988)
- 2.109 R. Lenormand, C. Zarcone: Phys. Rev. Lett. **54**, 2226 (1985)
- 2.110 S. Havlin, A. Bunde, J.E. Kiefer, unpublished (1991)
- 2.111 W. Kinzel, in: [2.3]
- 2.112 S. Redner: Phys. Rev. B **25**, 3242 (1982)
- 2.113 J.W. Essam, K. De'Bell, J. Adler: Phys. Rev. B **33**, 1982 (1986);
J.W. Essam, A.J. Guttmann, K. De'Bell: J. Phys. A **21**, 3815 (1988)
- 2.114 S.P. Obukov: Phys. Rev. Lett. **65**, 1395 (1990);
D.E. Wolf, J. Kertesz, S.S. Manna, S.P. Obukhov: Phys. Rev. Lett. **68**, 546 (1992)
- 2.115 M. Henkel, H.J. Herrmann: J. Phys. A **23**, 3719 (1990)
- 2.116 B. Hede, J. Kertesz, T. Vicsek: J. Stat. Phys. **64**, 829 (1991)
- 2.117 L.A.N. Amaral, A.-L. Barabási, S.V. Buldyrev, S.T. Harrington, S. Havlin, R. Sadr-Lahijany, and H.E. Stanley: Phys. Rev. E **51**, 4655 (1995)
- 2.118 M. Henkel, V. Privman: Phys. Rev. Lett. **65**, 1777 (1990)
- 2.119 P. Grassberger: J. Phys. A **22**, 3673 (1989);
J. Krug, J. Kertesz, D.E. Wolf: Europhys. Lett. **12**, 113 (1990)
- 2.120 P.L. Leath: Phys. Rev. B **14**, 5046 (1976)
- 2.121 J. Hoshen, R. Kopelman: Phys. Rev. B **14**, 3428 (1976)
- 2.122 J.M. Hammersley: Meth. in Comp. Phys. **1**, 281 (1963)
- 2.123 R.M. Ziff, P.T. Cummings, G. Stell: J. Phys. A **17**, 3009 (1984);
R.M. Ziff: J. Stat. Phys. **28**, 838 (1982)
- 2.124 R.M. Ziff: Phys. Rev. Lett. **56**, 545 (1986)
- 2.125 A. Weinreb, S. Trugman: Phys. Rev. B **31**, 2993 (1985)
- 2.126 Y. Gefen, A. Aharony, B.B. Mandelbrot, S. Kirkpatrick: Phys. Rev. Lett. **47**, 1771 (1981)
- 2.127 B.B. Mandelbrot, J. Given: Phys. Rev. Lett. **52**, 1853 (1984)
- 2.128 L. de Arcangelis, S. Redner, A. Coniglio: Phys. Rev. B **31**, 4725 (1985); Phys. Rev. A **34**, 4656 (1986)
- 2.129 A.S. Skal, B.I. Shklovskii: Sov. Phys. Semicond., **8**, 1029 (1975)
- 2.130 P.G. de Gennes: La Recherche **7**, 919 (1976)
- 2.131 D.S. Gaunt, A.J. Guttmann, in: *Phase Transitions and Critical Phenomena*, ed. by C. Domb, M.S. Green (Academic Press, New York 1974) p. 181
- 2.132 C. Domb, C.J. Pearce: J. Phys. A **9**, L137 (1976)
- 2.133 J. Adler: Computers in Physics **8**, 287 (1994)
- 2.134 P.J. Reynolds, H.E. Stanley, W. Klein: Phys. Rev. B **21**, 1223 (1980)
- 2.135 P.W. Kasteleyn, C.M. Fortuin: J. Phys. Soc. Jap. Suppl. **26**, 11 (1969)
- 2.136 H.K. Janssen: Z. Physik B **58**, 311 (1985)

